Experimental Investigation of Cavitation Using Refrigerant in a Two-Phase Flow System

by

Hatim Hamid Alrifaai

B.S., King Abdulaziz University, 2010

A THESIS

Submitted in partial fulfillment of the requirements for the degree

MASTER OF SCIENCE

Department of Mechanical and Nuclear Engineering
College of Engineering

KANSAS STATE UNIVERSITY
Manhattan, Kansas

2018

Approved by:

Major Professor
Dr. M. H. Hosni

Copyright

Abstract

Cavitation is a phase change process and its conversion of fluid from liquid to vapor requires pressure reduction. In this thesis, cavitation of R134a refrigerant is evaluated experimentally. This work is part of an ongoing project that seeks to develop a novel cooling cycle based on the cooling potential of the fluid during cavitation. A blowdown system was designed, built, and used for conducting the experiments. This system included a special test section containing a unique converging-diverging nozzle system designed for this investigation. In the end, cavitation was achieved by flowing the test fluid through a converging-diverging nozzle. As the fluid flows through the nozzle throat, the velocity increases while the pressure decreases and cavitation occurs when its static pressure drops below its vapor pressure. The onset of cavitation was evaluated by measuring pressure, temperature, and refrigerant flowrate, and by visualizing the flow using a high-speed video camera.

Table of Contents

List of Figures

List of Tables

Acknowledgements

I would like to thank those who have played a significant role in what I have accomplished. I am grateful to my parents for supporting my decision to study abroad. I highly appreciate my wife and children for their sacrifice, patience, and for helping me in my academic journey. My adviser, Dr. Hosni, supported me from day one of my graduate studies and guided me throughout. For this project, Dr. Eckles worked with me step-by-step in building the experimental system and designing the test section. Dr. Beck helped me with some calculation issues. The critical comments and valuable input of Dr. Sorenson impacted my work notably. Mr. Don Tomasi managed the project to keep it going. Mr. Garrett Mann helped me remarkably in setting up the experimental system. The technical experience of Mr. Eric Wagner was critical in building test sections. Mr. Zayed Ahmed introduced me to the high-speed video camera and trained me in its use. Mr. Malik Alkotami shared with me many useful technical articles that were used in this thesis. Mr. Luke Madden worked with me in the initial phase of building the system and helped me with the LabVIEW software.

Chapter 1 - Introduction

Vaporization is commonly known as a phase-change process, but there are two primary ways to convert a liquid to vapor. The first one is boiling which depends on increasing the temperature, while the second one is cavitation which depends on decreasing the pressure. Cavitation is usually considered as a problem that needs to be avoided in various industrial applications, but it may be used under controlled conditions to obtain positive outcomes. Frédéric Caupin and Eric Herbert [31] pointed out some natural phenomena and industrial applications which depend on the cavitation to be achieved.

The vaporization requires thermal energy to occur. For example, in boiling, the required thermal energy is obtained from an external heat source. On the other hand, in cavitation thermal energy is extracted from the fluid itself which causes a temperature drop. This phenomena inspired researchers to develop a novel cooling cycle by using cavitation to cause a temperature drop. The expected temperature drop grants the test fluid the potential of extracting heat from the ambient.

This thesis is part of a long-term project that seeks to create a cooling cycle that depends on the cavitation phenomena. To reach that goal, understanding the physics of cavitation is necessary. This thesis is a contribution in the investigation the cavitation of refrigerant R134a when it flows through a converging-diverging nozzle. The investigation was done experimentally, and the nozzle was designed to create the cavitation and allow visualization of the fluid's flow.

R134a, called Tetrafluoroethane, is a commonly used refrigerant. Figure 1.1 shows the molecular structure of R134a. The "R" symbolizes "refrigerant". The first digit refers to the number of carbon atoms (two) minus one, which leaves one. The second digit in R134a refers to

the number of hydrogen atoms (two) plus one, which equals three. The third digit in R134a refers to the number of fluorine atoms (three) plus one, which equals four. The letter "a" at the end indicates that another compound has the same components but in a different arrangement [1]. R134a is classified as A1 by ASHRAE. The "A" designation means the refrigerant is not toxic at concentrations of 400 ppm or less, while the "1" designation means it is not flammable when it is "tested in air at 21°C and 101 kPa." [1][2]

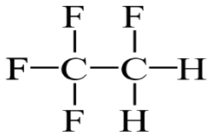

Figure 1.1 Molecular structure of R134a [3]

1.1 Definitions

In this section, the primary terminologies used in the thesis are defined.

Phase

"A phase is identified as having a distinct molecular arrangement that is homogeneous throughout and separated from the others by easily identifiable boundary surfaces." [4] The phases are solid, liquid and gas.

Phase change

Phase change is the transition of a substance from one phase to another.

Nucleation

Nucleation is the localized formation of a distinct thermodynamic phase. [5]

Vapor pressure

Vapor pressure is the saturation pressure at the given temperature. [6]

Cavitation

Cavitation is evaporation due to a pressure drop below vapor pressure. [6]

Boiling

Boiling is evaporation due to raising the fluid temperature to the saturation temperature.

Figure 1.2 illustrates the difference between cavitation and boiling. The figure is part of the phase diagram of water and the coexistence curve is shown in red.

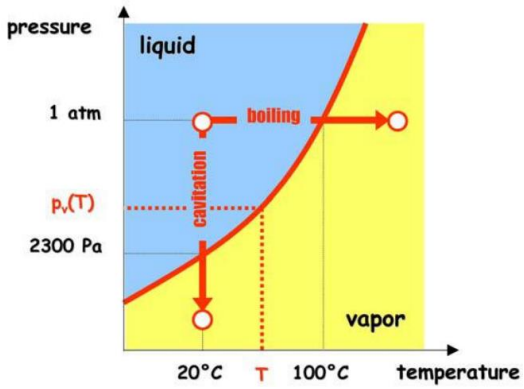

Figure 1.2 Difference between boiling and cavitation [32]

Homogeneous nucleation

Homogeneous nucleation is the "formation of the new phase solely from fluctuations within the old phase" [8].

Heterogeneous nucleation

"Heterogeneous nucleation begins on alien surfaces or particles, or pre-existing nuclei in the old phase. Dust or atmospheric aerosols can serve as heterogeneous nucleation centers for water condensation in the atmosphere." [8]

Cavitation inception

Cavitation inception is the cavitation onset.

Cavitation formation

Cavitation formation is the inception of cavitation.

Cavitation collapse

When the pressure outside a bubble is more than the pressure inside, the bubble will collapse. Figure 1.3 illustrates the bubble life stages that include formation, growth, and collapse.

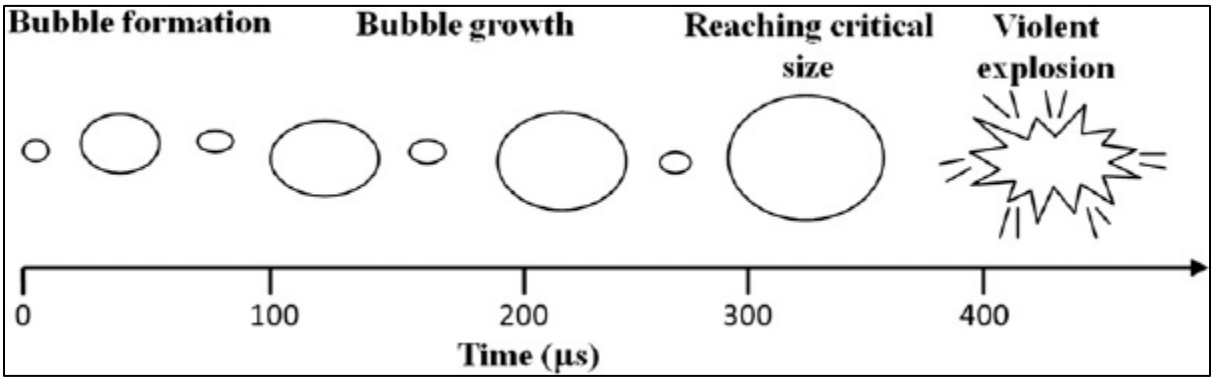

Figure 1.3 Bubble's life stages [9]

Phase diagram

The phase diagram is the "P-T diagram of pure substance." In the diagram, the "three phases are separated from each other by three lines" [4]. Figure 1.4 shows the phase diagram of water.

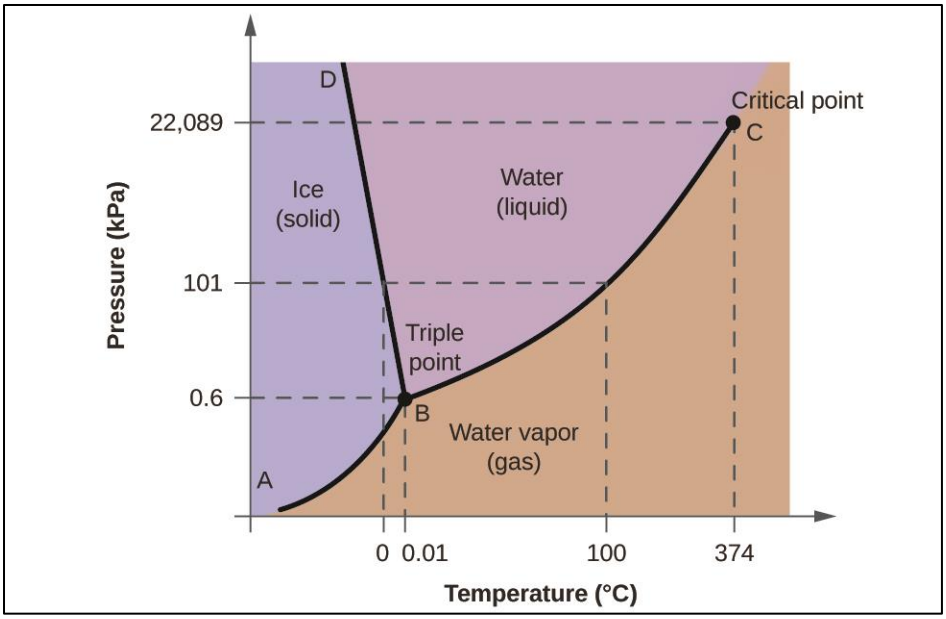

Figure 1.4 Phase diagram of water [10]

Coexistence curve

A coexistence curve is a curve that separates any two phases in the phase diagram. For example, the curve that separates liquid and vapor is a coexistence curve. Along the curve, liquid and vapor are in coexistence.

Degree of freedom

"The least number of intensive" properties "that must be specified to fix the values of all the remaining intensive" properties [14].

The degree of freedom might be 0, 1, or 2. It is 0 at the triple point, 1 at the coexistence curves and 2 at the other points in the phase diagram.

Metastable state

"Vapor that is supercooled below its equilibrium saturation temperature, and liquid that is superheated above its equilibrium saturation temperature, exist in a non-equilibrium condition referred to as a metastable state." [15]

Spinodal curve

Inside the saturation mixture region, the spinodal curve separates the unstable area from the metastable area.

Binodal curve

The binodal curve is the saturation curve. Figure 1.5 shows spinodal and binodal curves.

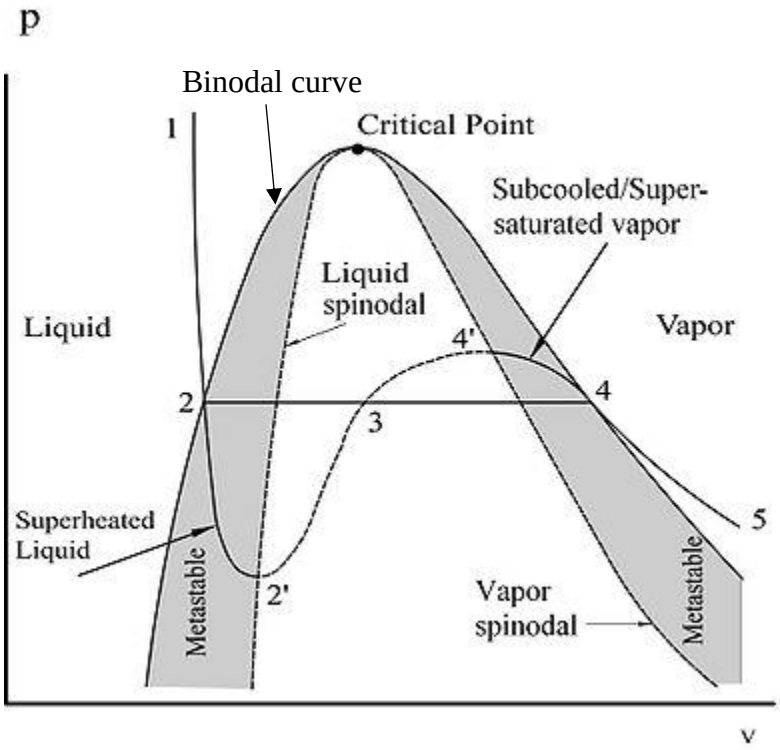

Figure 1.5 Illustration of spinodal and binodal curves [11]

Shock

A shock is the "sudden drop in velocity and a sudden increase in pressure" [4].

Void fraction

Void fraction is the "ratio of the gas flow cross-sectional area to the total cross-sectional area" [15].

$$\alpha = \frac{A_g}{A_g + A_l} \qquad (1.1)$$

Where:

A_g: The section area of the vapor

A_l: The section area of the liquid

Figure 1.6 illustrates void fraction. Green squares represent the vapor while white squares represent liquid.

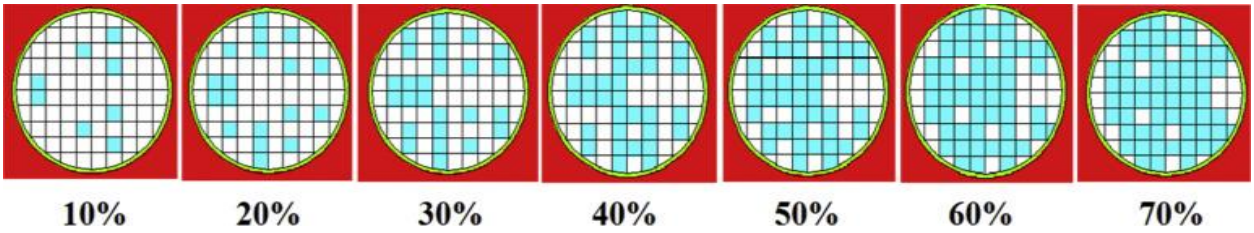

Figure 1.6 A schematic cross-sectional view of the void fractions for the bubbly regime from 10% to 70% [12]

Back pressure

Back pressure is the pressure applied to the downstream side of the converging-diverging nozzle.

Traveling bubble cavitation

"Weak points in the liquid, nuclei, grow from being almost invisible microscopic bubbles to being macroscopic bubbles when the pressure drops below the vapor pressure. Once the bubbles reach a region of sufficient pressure, they explosively collapse." [16]

Vortex cavitation

"In vortex cavitation, the pressure difference between the pressure side and the suction side results in a secondary flow going around the tip, which generates a vortex attached to the tip." [17]

Sheet/cloud cavitation

"Cloud cavitation is the formation and collapse of cavitation bubbles. It could develop from the shedding of cavitating vortices or a response to the disturbance forced on the flow. Cloud cavitation can be caused by the interference of a rotor and stator blades in a pump or turbine, and the contact between a propeller and a wake which created by the hull." [17]

Attached cavitation or sheet cavitation

"Attached cavitation is composed of cavities that are attached to the wall in a quasi-permanent manner. The attached cavitation shows variations in the flow pattern, with most of the fluctuations occurring near the end of the cavitation region." [16]

Free-energy barrier

The free-energy barrier is "The work of formation of a small embryo or nucleus of the new phase." [4]

Nucleation sites

Nucleation sites are the spots where the nucleation will take place.

Cavitation length

Cavitation length is the length of the cavitation region. Figure 1.7 illustrates the cavitation through a nozzle. The cavitation length in the first case is 15 mm while it is 30 mm in the second case.

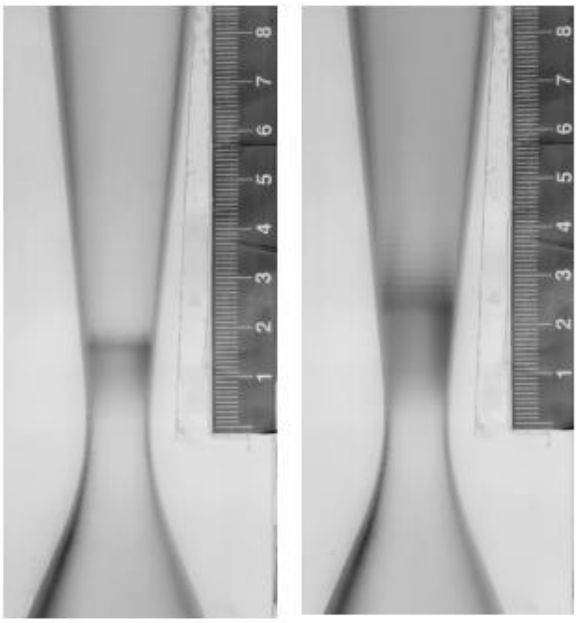

Figure 1.7 Cavitation through the nozzle [18]

Separated flow

"Separated flow consists of separate, parallel streams of two phases" [15]

Halogen

"Halogen element**,** any of the six nonmetallic elements that constitute Group 17 (Group VIIa) of the periodic table. The halogen elements are Fluorine (F), Chlorine (Cl), Bromine (Br), Iodine (I), Astatine (At), and Tennessee (Ts).

They were given the name *halogen*, from the Greek roots *hal-* ("salt") and *-gen* ("to produce"), because they all produce sodium salts of similar properties, of which sodium chloride—table salt, or halite—is best known." [21]

Organic halogen compounds

"Organic halogen compounds are a large class of natural and synthetic chemicals that contain one or more halogens (fluorine, chlorine, bromine, or iodine) combined with carbon and other elements." [22]

1.2 Literature Review

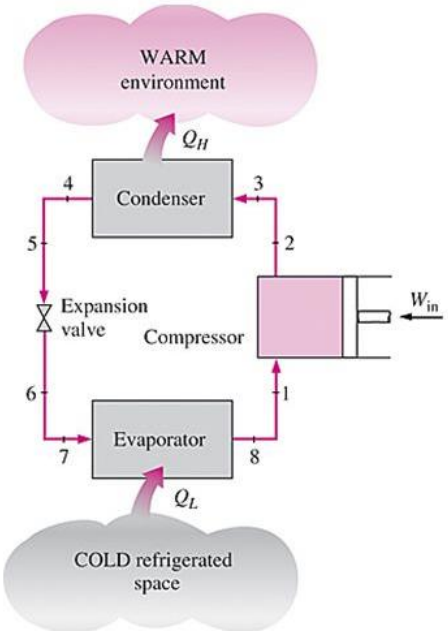

Figure 1.8 Schematic diagram of a vapor compression cycle [4]

The most common refrigeration cycle is the vapor compression cycle "due to its scalability, reliability, nontoxic and nonflammable refrigerants, use of electricity, and relatively compact size" [23]. As shown in Figure 1.8, the refrigerant at point 7 is two-phase liquid vapor mixure and its temperature is below the cooled space temperature. In the evaporator, heat is transferred from the cooled space to the refrigerant, which causes evaporation. At the inlet of the compressor (point 1), the refrigerant is a low-pressure vapor that will compress into a high-pressure vapor that has a temperature higher than the sink temperature. Inside the condenser, refrigerant will condense by conveying heat to the warm environment, and that process makes it a high-pressure liquid. The main function of the expansion valve is converting the refrigerant from a high-pressure liquid to a low-pressure mixture.

Because of Ozone depletion, the authorities that control the air conditioning industry have decided to phase out some refrigerants (e.g., R12) and to reduce using some other

refrigerants (e.g., R134a). In addition to that, other refrigerants that haven't negatively affected the Ozone layer are toxic (e.g., Ammonia) or flammable (e.g., 1234). Therefore, many researchers are working to develop alternatives to vapor compression cycle to get cooling cycles which are functional, safe, and harmless to the environment. William Goetzler and others presented several suggested cooling cycles in "Alternatives to vapor compression HVAC Technology." [2, 23]

Serguei Charamko [24] invented a cooling system that decreases the working fluid's temperature by flowing it through the converging-diverging nozzle. It is important to know that the temperature drop occurs when the pressure at the throat decreases below vapor pressure. At that point, the working liquid nucleates. The temperature drop occurs because the energy required to make bubbles is extracted from the liquid itself [25]. Figure 1.9 shows the system diagram. Table 1.1 contains the components of the cycle.

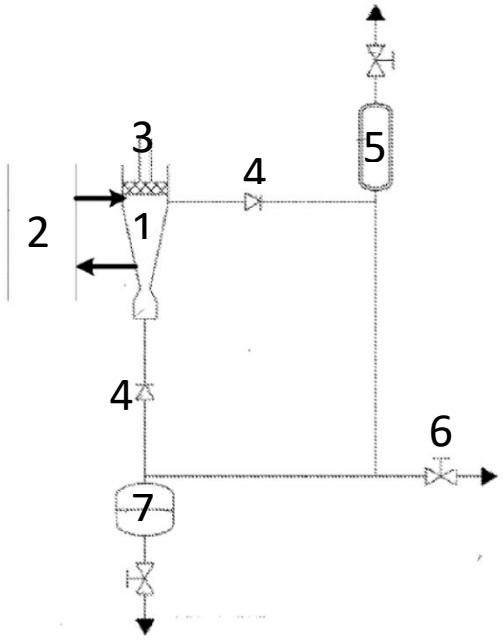

Figure 1.9 Critical flow refrigeration cycle [24]

Table 1.1 Critical flow refrigeration cycle components

	Components of the cycle
1	Converging-Diverging nozzle
2	Heat exchanger mechanism
3	Reciprocating piston
4	Check valve
5	Non-condensable gases trap
6	Charge-drain valve
7	Accumulator

Abdulmalik Alkotami and others [25] investigated the theoretical possibility of temperature drop due to cavitation for refrigerants R134a, R22, R123, and water. In addition to that, they drew the coexistence and spinodal curves for those refrigerants using two different equations of state. Equation 1.2 is an approximation of the predicted temperature drop due to cavitation. Figure 1.10 presents the predicted temperature drop for several refrigerants.

$$\Delta T = (\frac{\lambda h_{fg}(T_t)}{C_p/R})x \qquad (1.2)$$

Where:

$h_{fg}(T_t)$: Latent heat at the triple point

λ: The ratio of the latent heat of vaporization to its value at the triple point

C_p: Specific heat

R: Gas constant

x: Quality

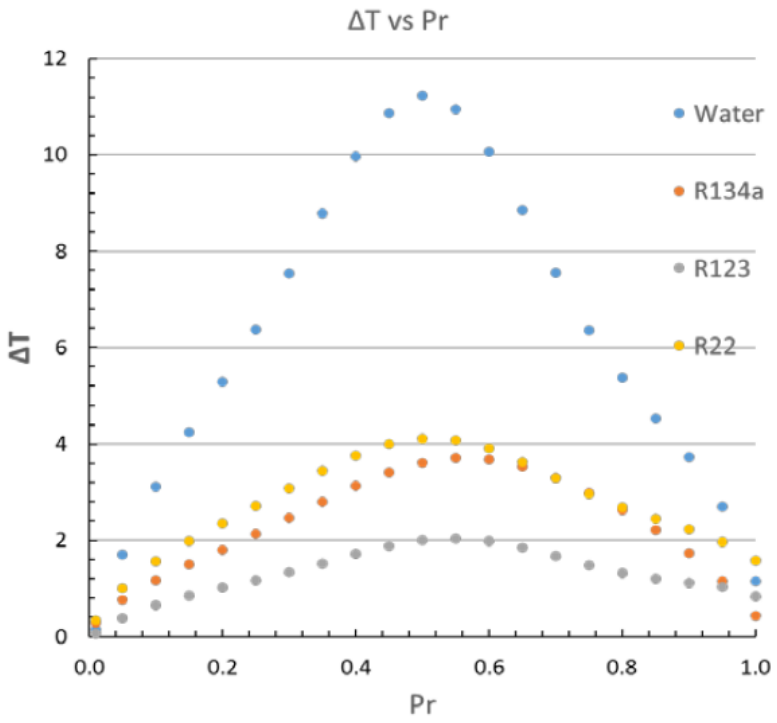

Figure 1.10 Temperature drop versus reduced pressure for water [25]

Cavitation occurs when the static pressure drops below the vapor pressure and conveys the fluid from the stable region to the metastable region. The metastable region is limited by two curves: coexistence and spinodal. The strength of cavitation is related to the degree of metastability.

Using the Peng-Robinson Equation of State, Alkotami calculated the coexistence and spinodal curves for R134a as shown in Figure 1.11. Because the top point of the spinodal curve and the critical point should be identical, he shifted the spinodal curve by multiplying the spinodal data by 1.17. The coexistence and shifted spinodal curves are shown in Figure 1.12.

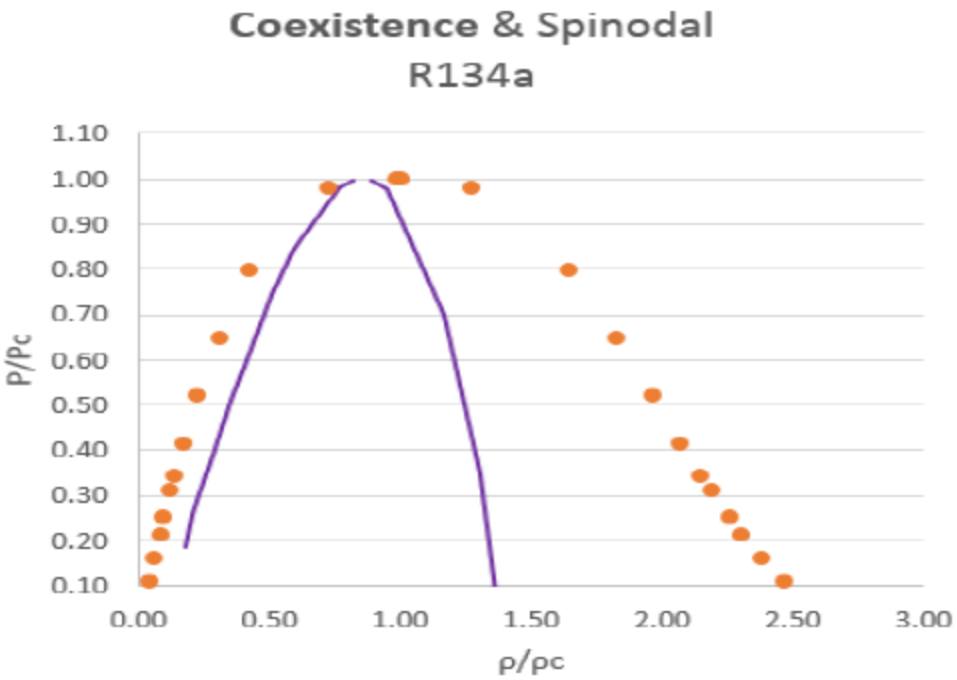

Figure 1.11 Coexistence and spinodal curves (reduced pressure vs. reduced density) for R134a [25]

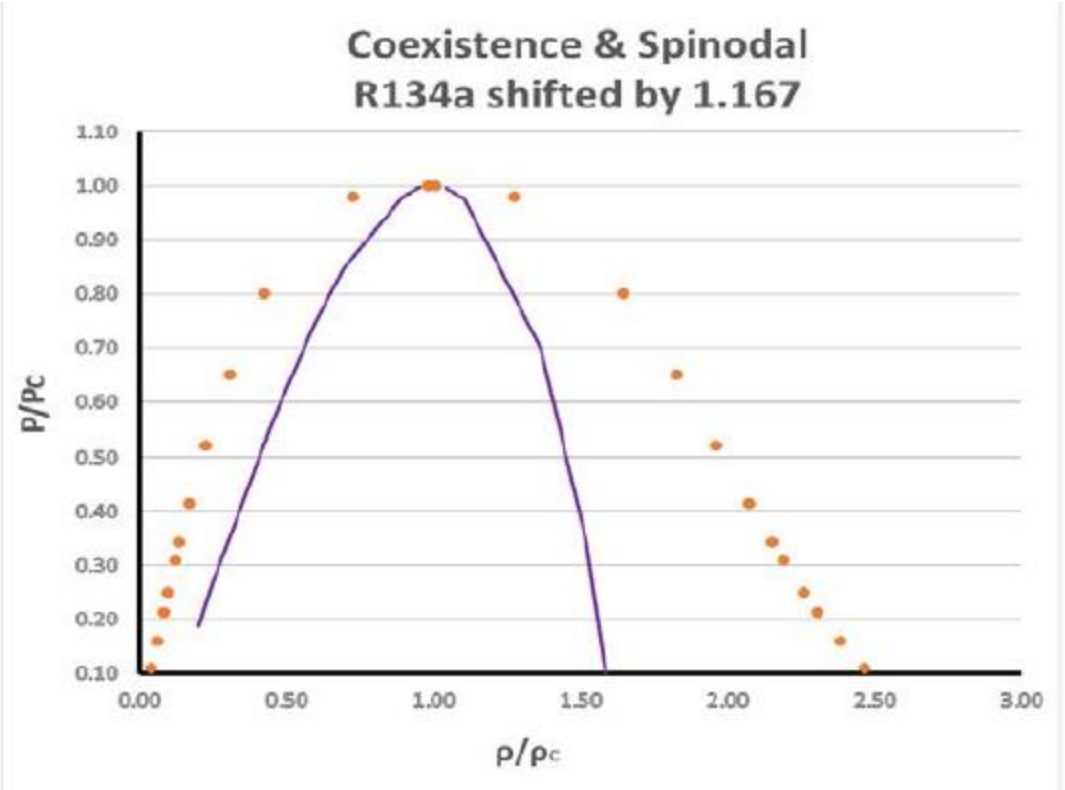

Figure 1.12 Coexistence and shifted spinodal curves (reduced pressure vs. reduced density) for R134a [25]

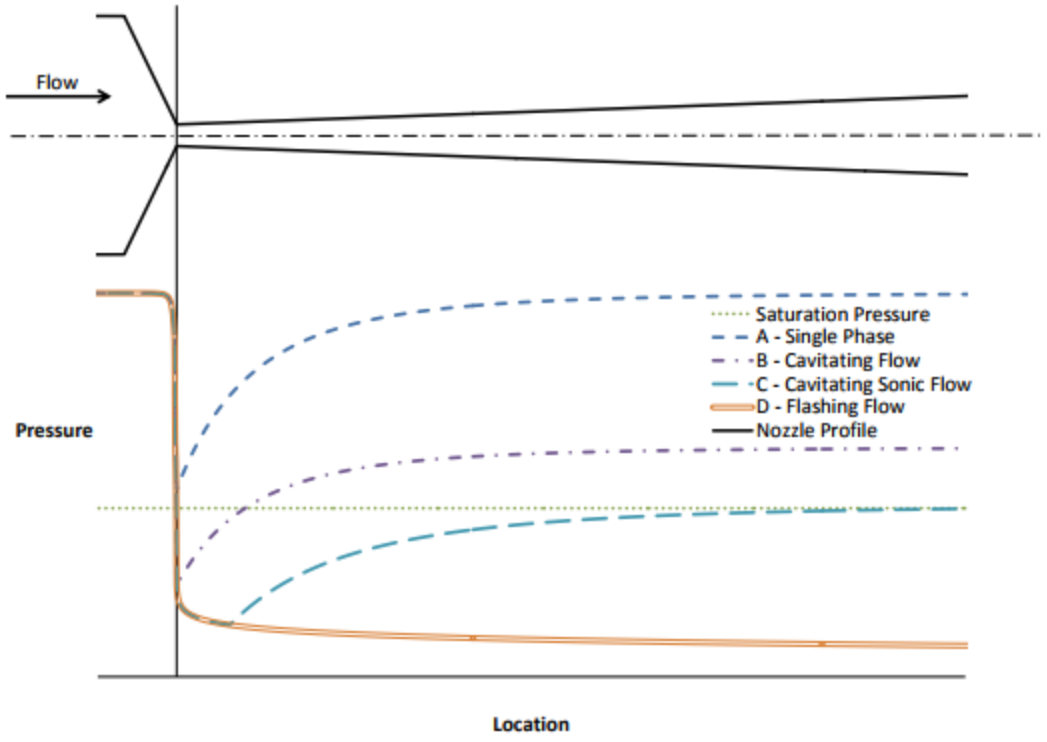

Figure 1.13 Nozzle pressure distribution by flow type [26]

William Asher [26] explained the suspected flowing behavior of the subcooled liquid when it flows through the converging-diverging nozzle. Figure 1.13 illustrates these situations. At the upstream side, the liquid is subcooled and its pressure is far away from the saturated pressure, which is also called vapor pressure. At the throat, the velocity increases and, consequently, the pressure decreases. In case A, the pressure decreases but it stays above the saturation pressure, so it doesn't vaporize. In contrast, throat pressures for cases B, C, and D drop below the saturation pressure, so vaporization will take place. To express the difference between cases B, C, and D, the local pressure drops below saturation pressure for case B, but the pressure will increase directly because of the gradual increasing of the section area since the flow is not sonic. For case C, the flow is sonic, so the pressure will continue to decrease but for a

small distance. For case D, the flow is supersonic, so the pressure will decrease or remain constant for a long distance even as the section area increases.

To investigate the local sonic velocity of R134a, Graham Wallis [27] presented an equation (1.3) that gives the local sonic velocity according to the void fraction. Figure 1.14 shows the variation of the sonic velocity of R134a at 25°C according to Equation 1.3.

$$C^2 = [(\alpha\rho_g + (1-\alpha)\rho_f)(\frac{\alpha}{\rho_g C_g^2} + \frac{1-\alpha}{\rho_f C_f^2}]^{-1} \qquad (1.3)$$

Where:

C: Sonic velocity

α: Void fraction

ρ_g: Vapor density

ρ_f: Liquid density

C_g^2: Vapor sonic velocity

C_f^2: Liquid sonic velocity

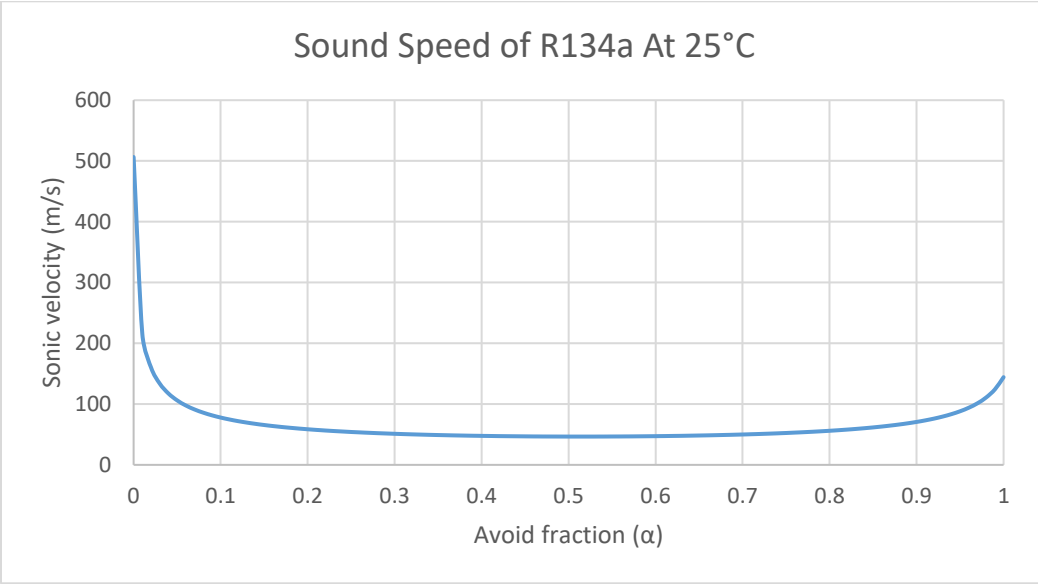

Figure 1.14 Sound speed of R134a at 25°C

Yves Lecoffre [28] discussed the dimensionless parameters that indicate the cavitation phenomenon. The main dimensionless number that relates to cavitation is the cavitation number (σ), which is defined in Equation 1.4.

$$\sigma = \frac{P_{up} - P_v}{\frac{1}{2}\rho V_{up}^2} \qquad (1.4)$$

Where:

P_{up}: Upstream pressure

P_v: Vapor pressure

ρ: density

V_{up}: Velocity

Regarding this cavitation number, Lecoffre stated

> "Equality of σ of cavitation in two geometrically similar flows signifies that if the vapor pressure is attained, it does so at two homologous points. Contrary to what is often implicitly assumed, σ of cavitation is not strictly a parameter of simulated of cavitating fluids. All it does is facilitate determination of the level of the absolute pressure compared to the vapor pressure at all points of a non-cavitating flow. In particular, to define σ in the performance of a machine, it is not essential that occur in it. If the value of σ is sufficiently large, cavitation may not appear at all."

The pressure coefficient (C_p) is another dimensionless number that clarifies the flowing situation. It is defined in Equation 1.5.

$$C_p = \frac{P_t - P_{up}}{\frac{1}{2}\rho V_{up}^2} \qquad (1.5)$$

Where:

P_t : Pressure at throat

P_{up}: Upstream pressure

ρ: Density

V_{up}: Upstream velocity

Lecoffre expressed that comparing the cavitation number and $(-C_p)$ can act as a guide to a cavitation prediction. There are three states of the numbers:

1- $\sigma > -C_p \Leftrightarrow P_t > P_v \Leftrightarrow$ no cavitation

2- $\sigma = -C_p \Leftrightarrow P_t = P_v \Leftrightarrow$ on the coexistence curve

3- $\sigma < -C_p \Leftrightarrow P_t < P_v \Leftrightarrow$ Cavitation area

Zayed Ahmed [29] conducted experiments that included water flowing through a converging-diverging nozzle. One of his observations was that the water needs enough of a pressure drop below the saturation pressure to cavitate. Depending on his experiments, the water pressure at the throat should decrease at least 20 kPa below the saturation pressure to create cavitation.

1.3 Objectives

1.3.1 Investigation of cavitation inception

The researcher sought to investigate where the cavitation started depending on the recorded videos. The goal was deciding whether the cavitation begun at the throat, after the throat or before it. Also, the required pressure drop for cavitation, needed to be investigated. The pressure drop in this context means the quantity of pressure drop below the vapor pressure. The question that should be answered, was any pressure drop caused cavitation or it should be more than certain number to caused cavitation. To investigate

the cavitation, there were several non-dimensional numbers that were used to predict the cavitation possibility and to describe the flow.

1.3.2 Observation the impact of upstream pressure and throat area on the cavitation

The experiments are accomplished with different upstream pressures and two nozzles, which have different throat areas. To understand the physics of the cavitation, observation of the impact of the upstream pressure and throat area are necessary.

Chapter 2 - Experimental Test Facility, Measurement Equipment, and System Setup

This chapter presents the apparatus that was used to conduct onset cavitation test, and how to operate it. Detailed explanation about the blowdown system is offered in this chapter to demonstrate its parts and their functions. The test section is highlighted to clarify how it was designed. Because the system's operation is complicated, the operation procedure is expressed at the end of the chapter.

2.1 Blowdown System

To accomplish the experiments, a blowdown system was built. Figure 2.1 illustrates a schematic of the system and Table 1 presents the system's components. A photograph of the system is shown in Figure 2.2.

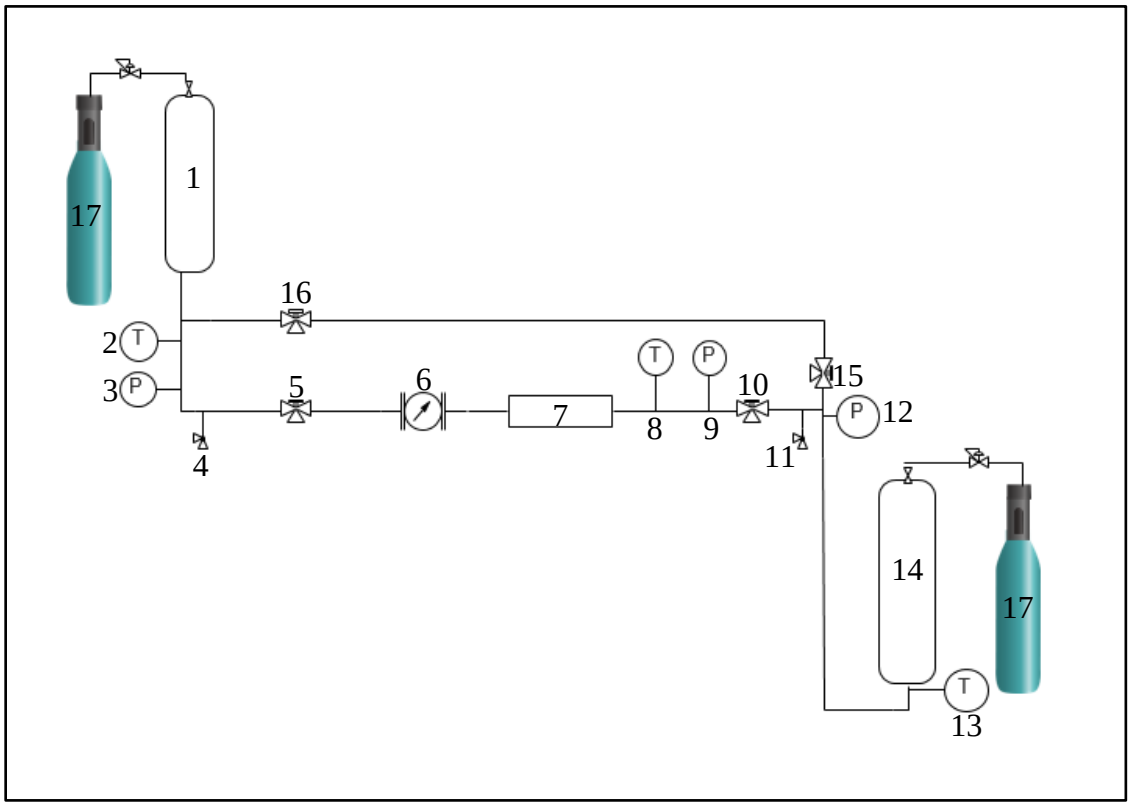

Figure 2.1 Blowdown system diagram

Table 2.1 System's parts

Number	Part name
1	Upstream accumulator
2	Upstream pressure transducer
3	Upstream thermocouple
4	Safety valve
5	Valve #4
6	Flowmeter
7	Test section
8	Downstream thermocouple
9	Downstream pressure transducer
10	Valve #1
11	Safety valve
12	Back pressure transducer
13	Thermocouple
14	Downstream accumulator
15	Valve #2
16	Valve #3
17	Nitrogen cylinder

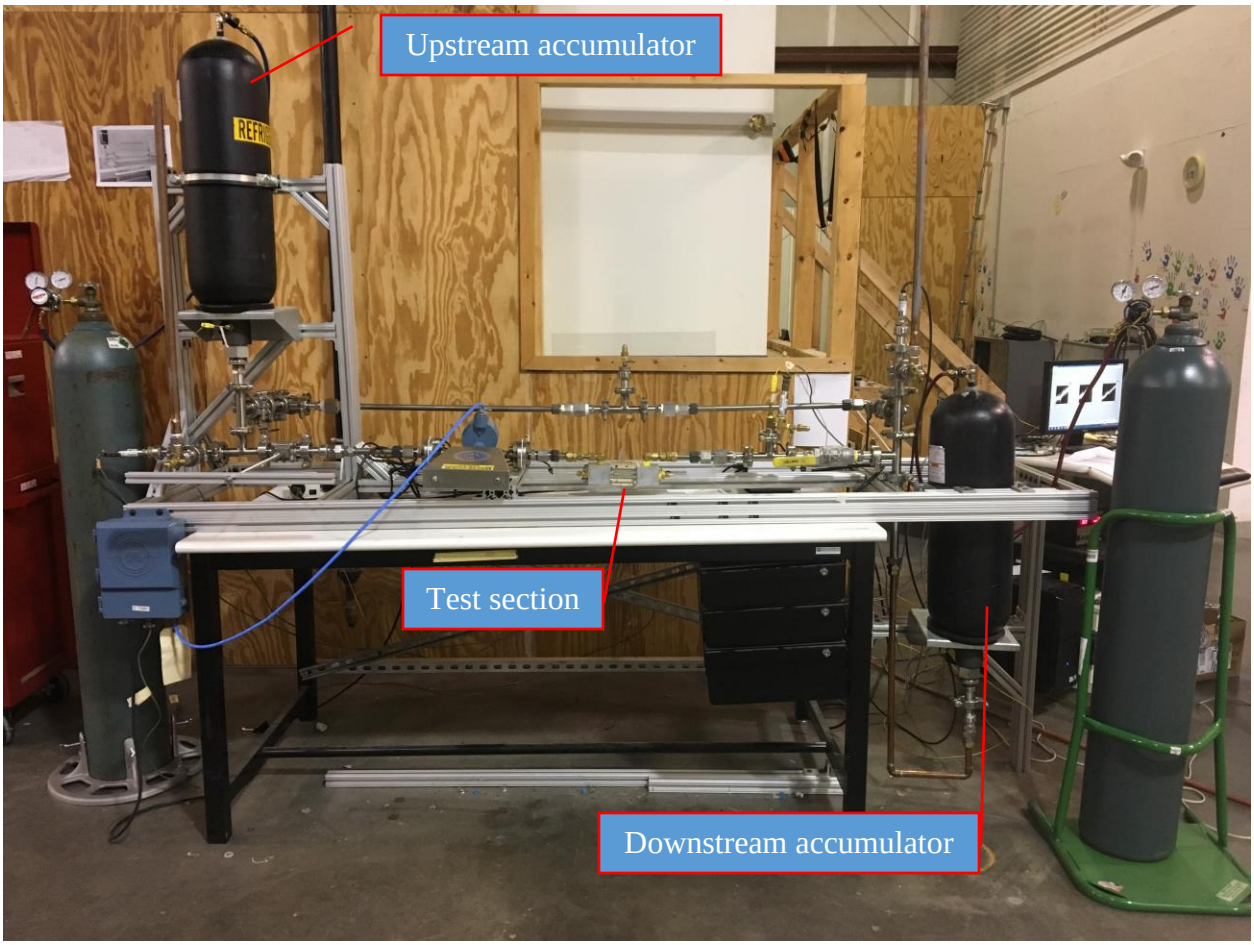

Figure 2.2 Blowdown system

In the blowdown system, the upstream pressure and downstream pressure were controlled by the upstream accumulator and downstream accumulator. The accumulators control the pressure of the system by increasing and decreasing the quantity of nitrogen in an internal bladder. Figure 2.3 shows a sectional view of the accumulator. The figure illustrates the working principle of the accumulator.

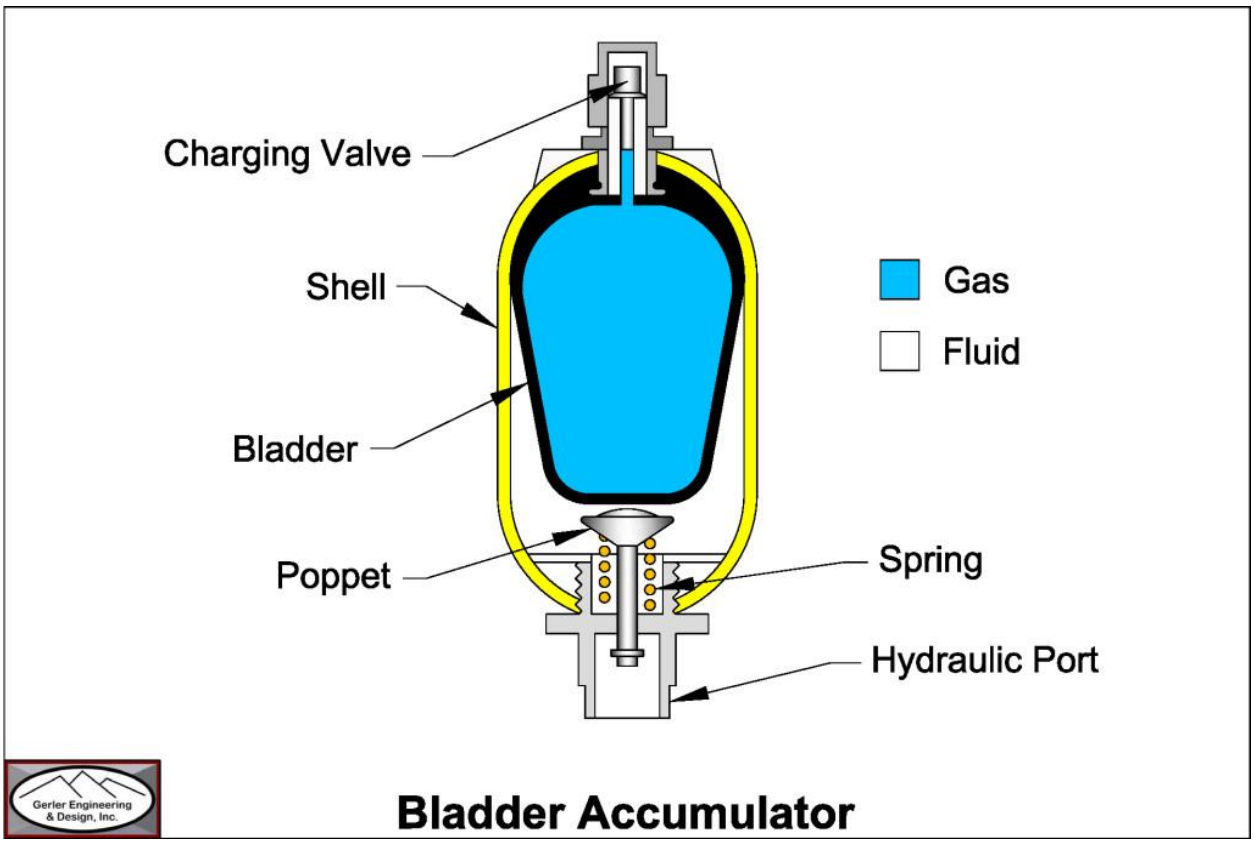

Figure 2.3 Sectional view of an accumulator [30]

2.1.1 Flowrate measurement

To measure the mass flow rate, a flowmeter was installed at the upstream side where the working fluid (R134a) is liquid. The brand of the selected flowmeter was Micro Motion and its model number was DS040S113SU. It converted the flowrate to an electrical current in the range 4 mA to 20 mA. Figure 2.4 shows photograph of the flowmeter used.

Figure 2.4 The mass flowmeter

2.1.2 Temperature measurement

Type K thermocouples were used to measure the temperature at three locations. The first was on the upstream line. The second thermocouple was on the downstream side, and the third thermocouple was on the back pressure zone. All of the thermocouples were immersed inside the tubes and measured the refrigerant temperature directly.

2.1.3 Pressure measurement

In the blowdown system, there were three pressure transducers. One measured the upstream pressure and the second one measured the downstream pressure. The third one was for the back pressure zone. Each one of the pressure transducers measured the pressure as an electrical voltage in the range of (0 – 5 V dc).

2.1.4 Data acquisition system

To collect the measured data and display them as meaningful values, a Data Acquisition System (DAQ) was used. To get the benefits from the DAQ, LabVIEW software was required. A LabView file was designed for the blowdown system to do five tasks. The first one was

converting the electrical voltage that transmits from the pressure transducer to pressure in psi. The second task is converting the electrical current that transmits from the flowmeter to mass flow rate in kg/s. The third task is converting the electrical voltage that transmits from the thermocouple to temperature in °C. The fourth function is displaying the measured values. The fifth is recording the measured valued in separated files. Figure 2.5 is the block diagram of the LabView file and Figure 2.6 is the front panel of it.

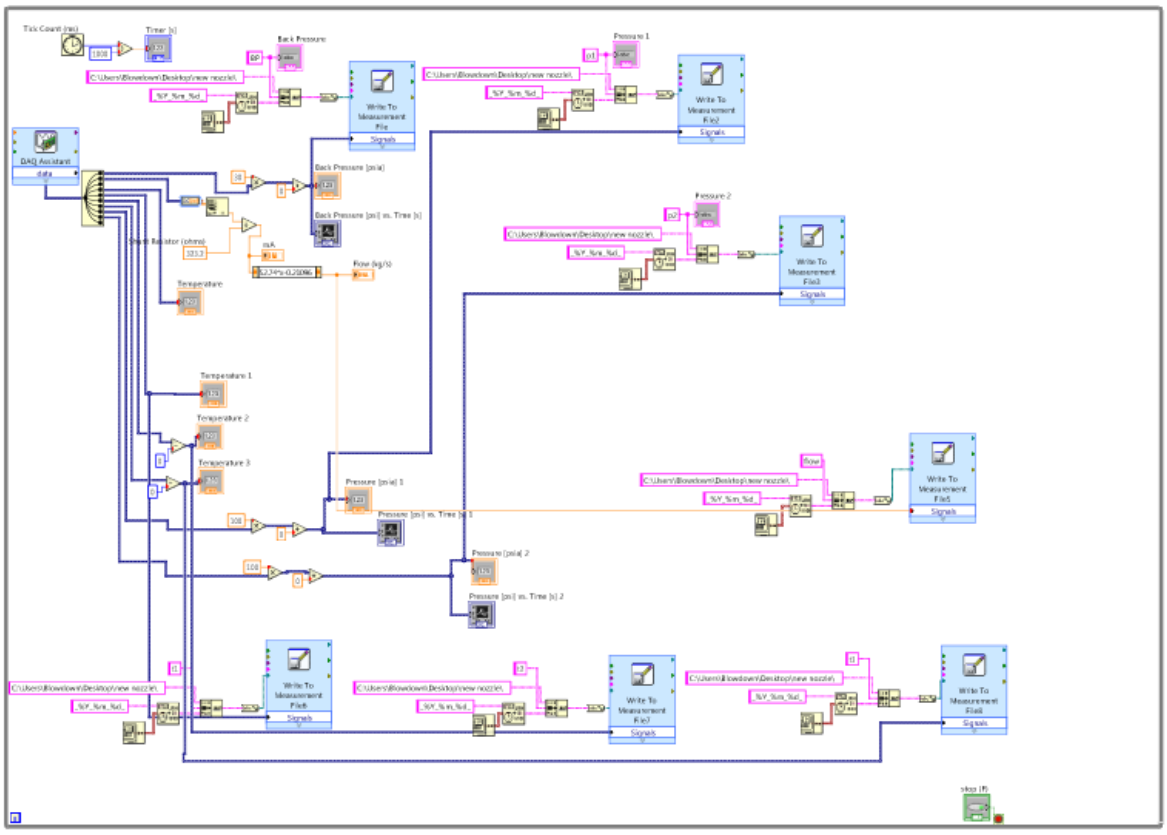

Figure 2.5 Block diagram of the LabView file

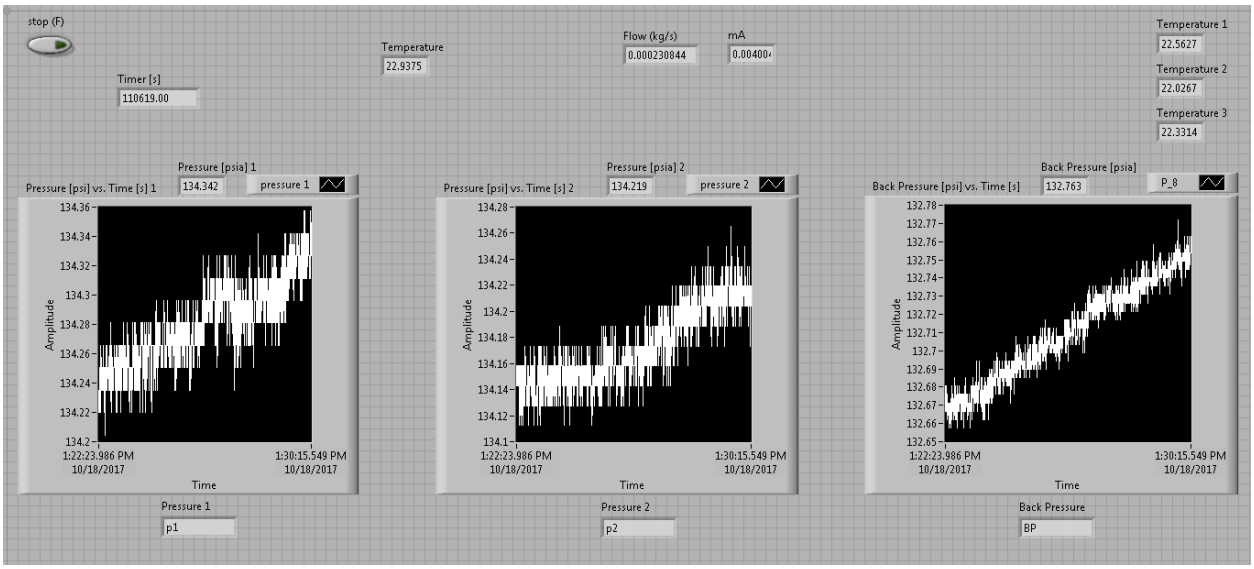

Figure 2.6 Front panel of the LabVIEW file

2.2 Test Section

To accomplish the research objectives, designing a proper test section was critical. The test section needed to obey four conditions. First, it had to be transparent so the camera could record what was happening inside. Second, it needed to be compatible with R134a. Third, it had to be workable with high pressure (more than 300 psi). The fourth condition was that it needed to be sealed. Figure 2.7 shows the assembly drawing of the test section, while Figure 2.8 is the section view of it. The drawings were done using the Solidworks software. The test section contained 12 parts, which are listed in Table 2.2.

Table 2.2 List of test sections parts

Part name	Part quantity
Glass tube	1
Cup	2
Bored-Through Male Connector	2
Elbow	2
O-ring	2
Teflon ring	2

The insert	1

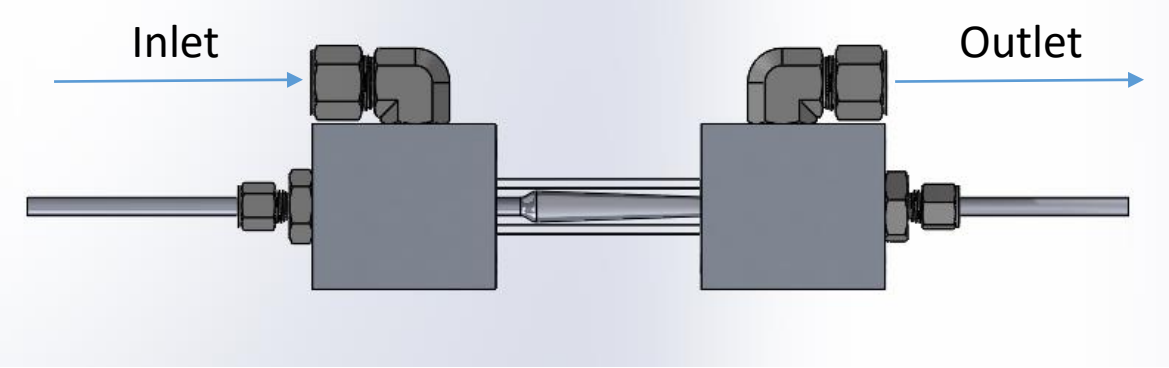

Figure 2.7 Assembly drawing of the test section

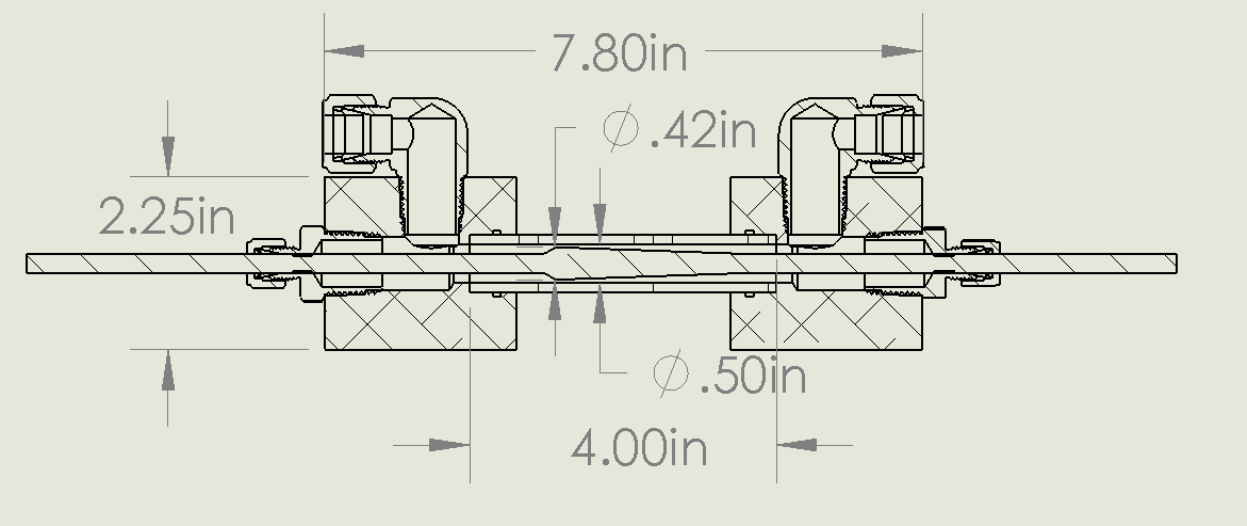

Figure 2.8 Sectional view of the test section

2.2.1 Description of each part of the test section

2.2.1.1 Glass tube

The glass tube used was made of borosilicate glass and it was selected because it was compatible with R134a and workable with high pressure. The length of the tube was 4 inches

and its inner diameter was 0.5 inches, while its outer diameter was 0.75 inches. The tube was made by the Gauge Glass Company.

2.2.1.2 Cup

The cups were the two parts that connected together the tube, the elbows, the Bored-Through Male Connector, and the insert. They were designed by the author and made by the Mechanical and Nuclear Engineering Department shop at Kansas State University. The critical issue was selecting the correct dimensions for the O-ring's groove. The groove's dimension depended on a specific standard shown in Appendix B. Figure 2.9 is the 3D drawing of the cup and Figure 2.10 is the section view. Figure 2.11 is the cup's drawing, showing its dimensions.

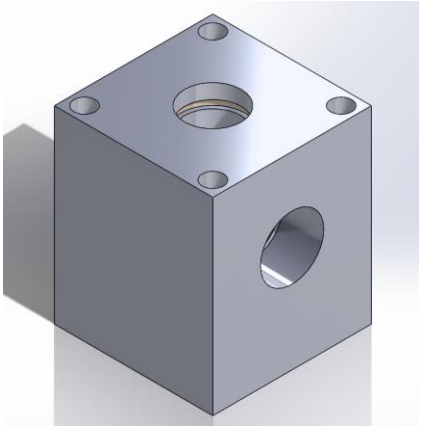

Figure 2.9 3D drawing of the cup

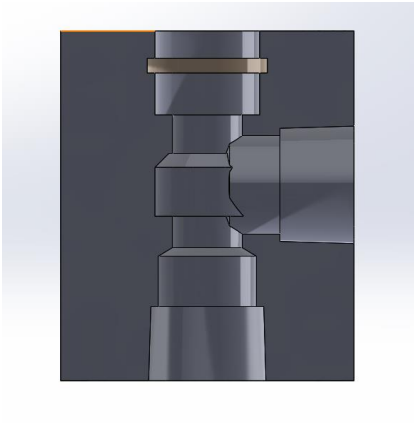

Figure 2.10 Sectional view of the cup

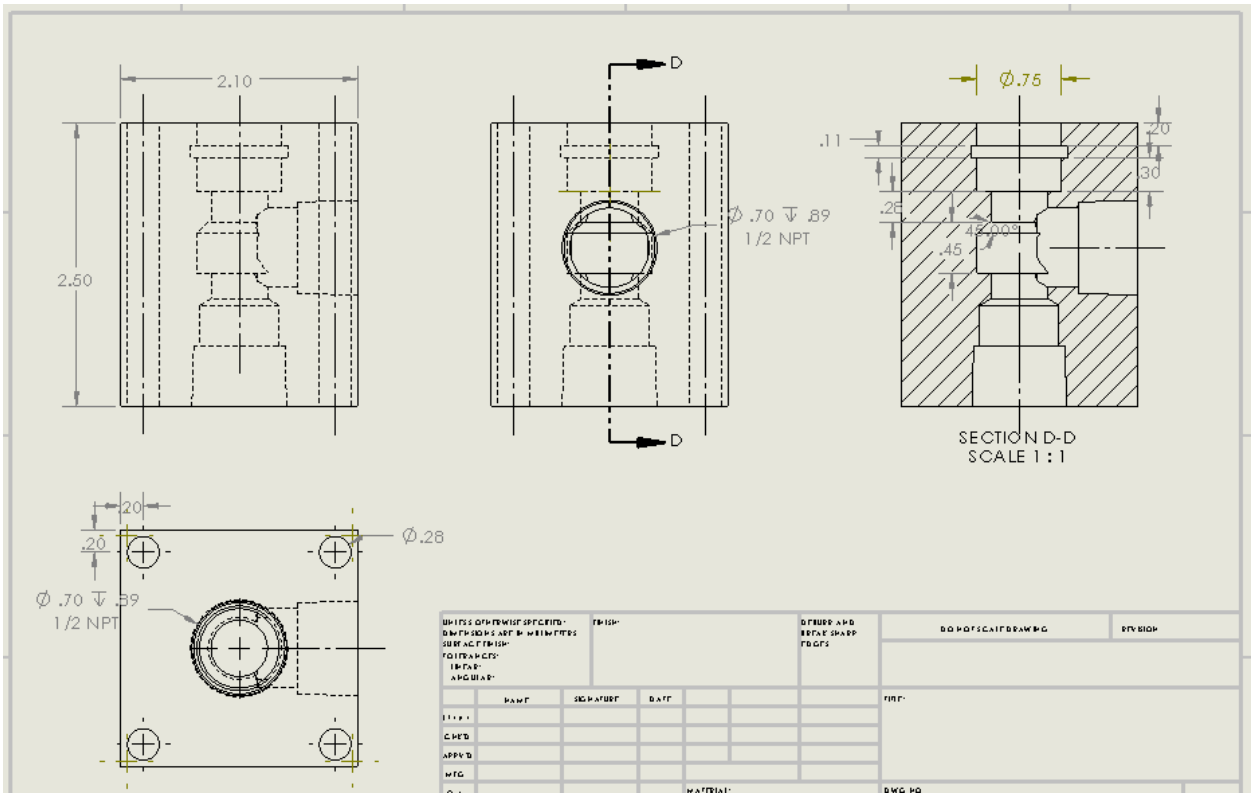

Figure 2.11 Drawing sheet of the cup

2.2.1.3 Elbow

The test section needed an elbow as an inlet and another one as an outlet. The selected elbow was a ½ inch Swagelok brass tube fitting. Figure 2.12 is the elbow tube fitting used.

Figure 2.12 Elbow tube fitting

2.2.1.4 Bored-through male connector

To fix the insert, two bored-through male connectors were required. A ¼-inch brass Swagelok fitting was selected. Figure 2.13 shows a photograph of the bored-through male connectors used.

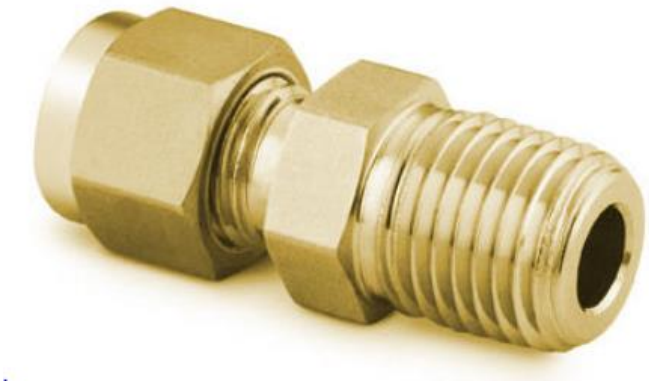

Figure 2.13 Bored-through male connector

2.2.1.5 O-ring

To avoid refrigerant leakage between the cup and the glass tube, using a proper O-ring was necessary. The selected O-ring's material was Nitrile, which is compatible with R134a. Figure 2.14 illustrates the O-ring selection procedure.

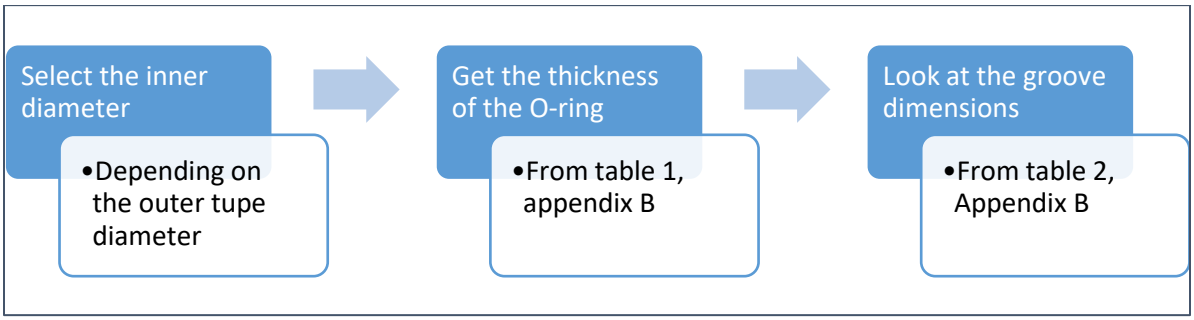

Figure 2.14 O-ring selection procedure

2.2.1.6 Teflon ring

At the contact area between the metal cup and the glass tube, adding a Teflon ring is necessary to avoid cracking of the glass due to direct contact between the glass and metal. The Teflon was also compatible with R134a.

2.2.1.7 The insert

The insert, made of aluminum, were responsible for changing the crossectional area of the flowing zone inside the glass tube, creating a converging-diverging nozzle geometry. In this project, two inserts were tested. The throat diameter of the first one was 0.42 inches and is referred to in this thesis as "Nozzle #1" (see Figure 2.15). The second insert had a throat diameter of 0.435 inches and is referred to as "Nozzle #2."

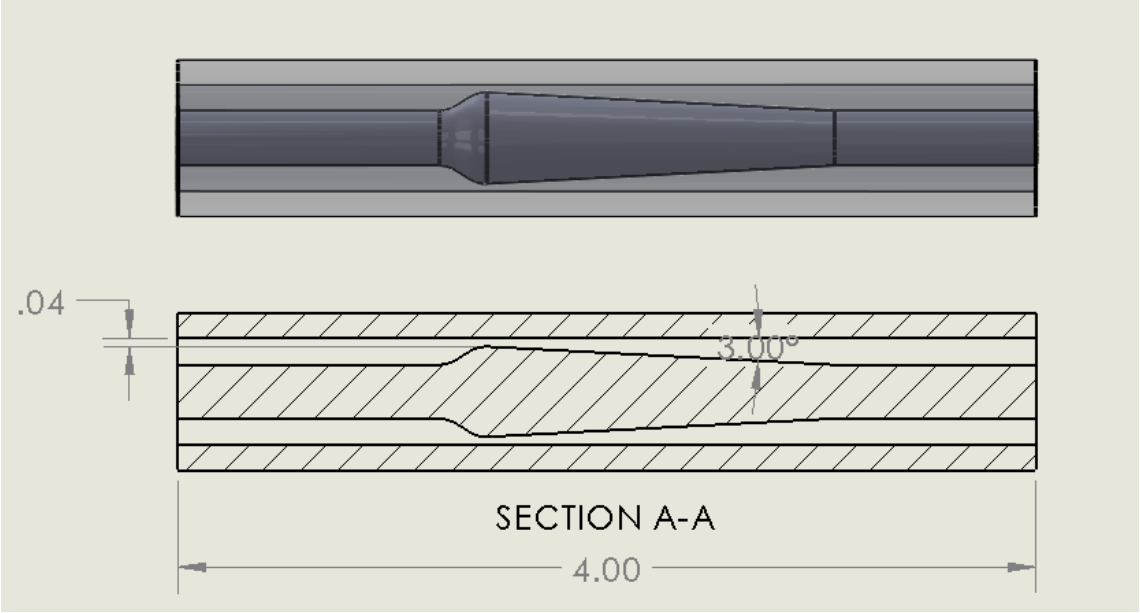

Figure 2.15 Nozzle #1

2.2.2 Hydraulic test

After assembling the test section, testing its compatibility with high pressure was an important issue. Accordingly, a hydraulic test was performed by pumping water to the test

section with a manual pump. At the beginning of the hydraulic test, the test section was pressurized to 250 psig. Then, the pressure was increased in steps of 50 psi. At the end of the test, the pressure was 500 psig. Figure 2.16 shows a photograph of the hydraulic test setup and Figure 2.17 shows the pressure at each stage of the hydraulic test. According to the test, the test section was compatible with 500 psig.

Figure 2.16 Hydraulic test setup

Figure 2.17 The pressure of each stage of the hydraulic test

2.2.3 Leakage test

Before using the test section, a leakage test was required. To do the test, the test section was connected to the nitrogen tank by a hose, and a pressure transducer was installed to measure the pressure inside the test section. At the beginning of the test, the pressure was 65.58 psi while

it was 65.44 after 24 hours. That means the pressure drop rate was 0.7 Pa/minute, which means that the test section is sealed. Figure 2.18 shows the leakage test setup.

Figure 2.18 Leakage test setup

2.3 High-Speed Camera

A high-speed camera was necessary to record the experiments clearly. A Photron SA5 High-Speed Camera was used in the experiments to visualize the cavitation inside the test section. This camera allowed the user to select the suitable zoom, resolution, and the frame rate (number of frames per second). To use the camera, the user needed to upload software called "Photron Fastcam Viewer," which allowed the user to control the video specifications. The camera used is shown in Figure 2.19.

Figure 2.19 The high-speed camera

2.4 Fiber Optic Halogen Light

The high-speed camera needed more light than an ordinary camera. The light should be steady and high-intensity. In this system, two fiber optic halogen light sources were used. One was on the front side and the other was on the back side. To get a diffused light, a paper sheet was added in front of the back side light. The fiber optic halogen light sources used are shown in Figure 2.20 and 2.21. Figure 2.22 is the top view of the test section to illustrate the lighting setup.

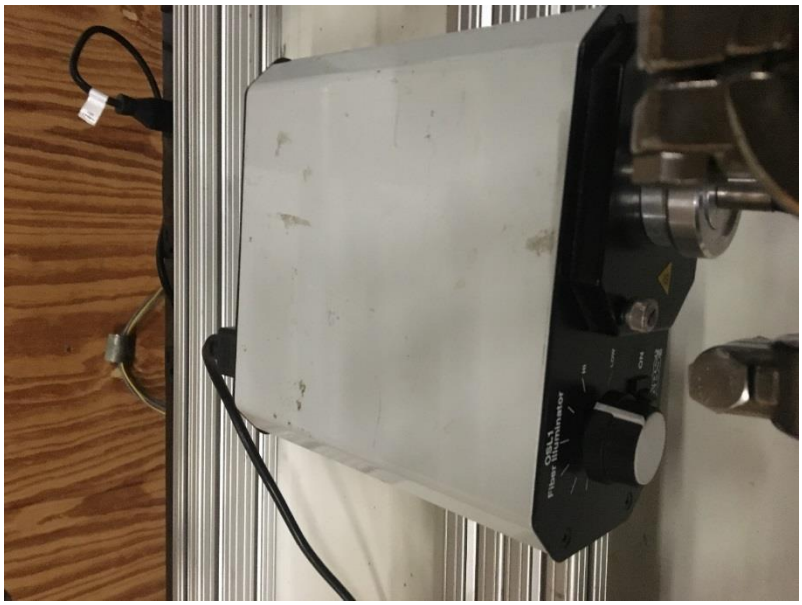

Figure 2.20 Fiber optic halogen light source

Figure 2.21 Fiber optic halogen light source

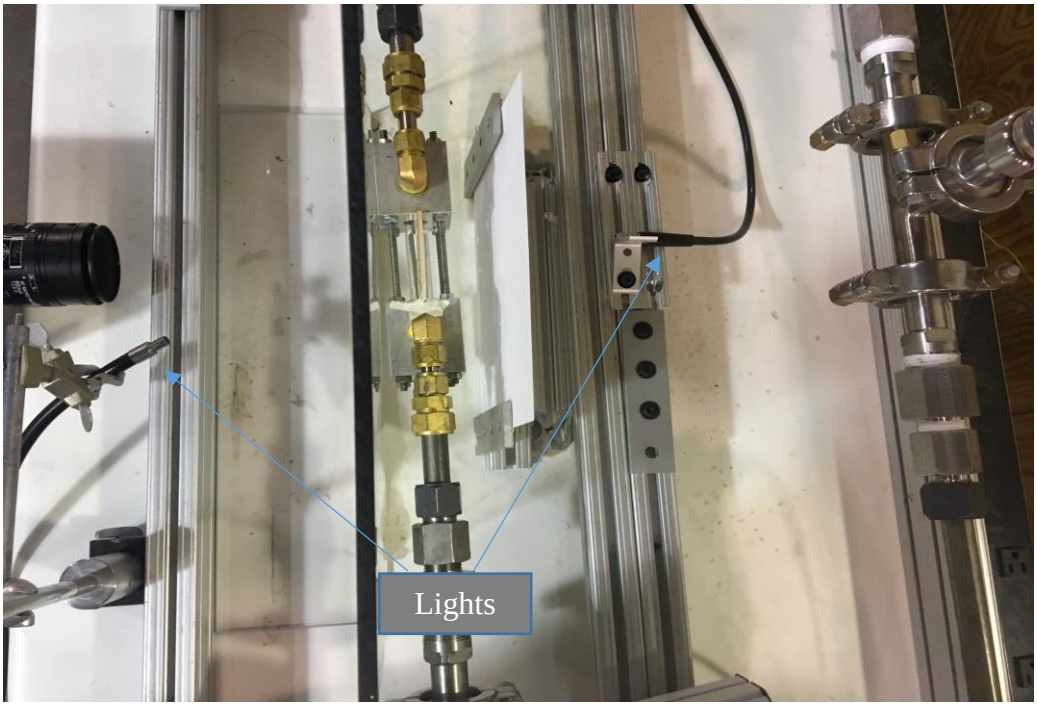

Figure 2.22 The top view of the test section to illustrate the lighting setup

2.5 Safety Aspects

Because the system worked with high pressures, safety was a serious issue; therefore, two relieve valves were installed. They were there to protect the system if the pressure exceeds 500 psia. A transparent shield was placed in front of the test section to protect the operator and the camera if the glass were to break. In addition, each nitrogen cylinder had a standalone holder to prevent it from falling.

2.6 Operational Procedure

To run the system, a specific procedure was followed. It is explained below.

2.6.1 Preparing the high-speed camera

In the beginning, adjusting a suitable video setting was required. To get a clear recording, the front light and back light were confirmed to be at the appropriate position. Also, three settings needed to be checked: zoom, resolution, and number of frames per second. The zoom was controlled by manually adjusting the lens until a clear view was shown on the Photron

Fastcam Viewer. The required resolution depended on the spot that needed to be examined and was set by the Photron Fastcam Viewer. Setting the number of frames per seconds depended on the required resolution and on the available light because increasing the number of frames requires an increase in the light intensity.

2.6.2 Collecting the refrigerant in the upstream

Before beginning the experiment, the refrigerant was evacuated from the back pressure side and collected at the upstream side. This was accomplished in several steps. First, valve #1 was closed and valve #2 was opened. Second, the pressure at the upstream bladder was set at 100 psig, which was accomplished by releasing Nitrogen from the bladder. Then, the pressure of the downstream bladder was increased to 150 psig by adding more Nitrogen from the cylinder. Finally, valve #2 was closed to get two separated zones: upstream side and back pressure side. Launching the LabVIEW file was necessary to check the pressures and temperatures of the system.

2.6.3 Setting the required upstream pressure and back pressure

The pressure of the downstream bladder was decreased by releasing nitrogen until it arrived at a pressure right above the saturation pressure at that time because if the pressure arrives at the saturation pressure and goes below it, the refrigerant will vaporize and the vapor pressure will be more than the bladder pressure. In that case, the nitrogen will escape from the bladder, causing it to collapse and potentially crack. Deciding the required upstream pressure depended on the pressure that needed to be tested, and getting that pressure was accomplished by adding more Nitrogen to the upstream bladder.

2.6.4 Running the experiment

The camera specifications were rechecked at this stage to be sure that everything was at the required setting. To run the experiment, valve #1 was opened and the video recording was started at the same time. The experiment was done when the the measured data of the three pressure transducer were equaled. Figure 2.23 summarizes the operational procedure.

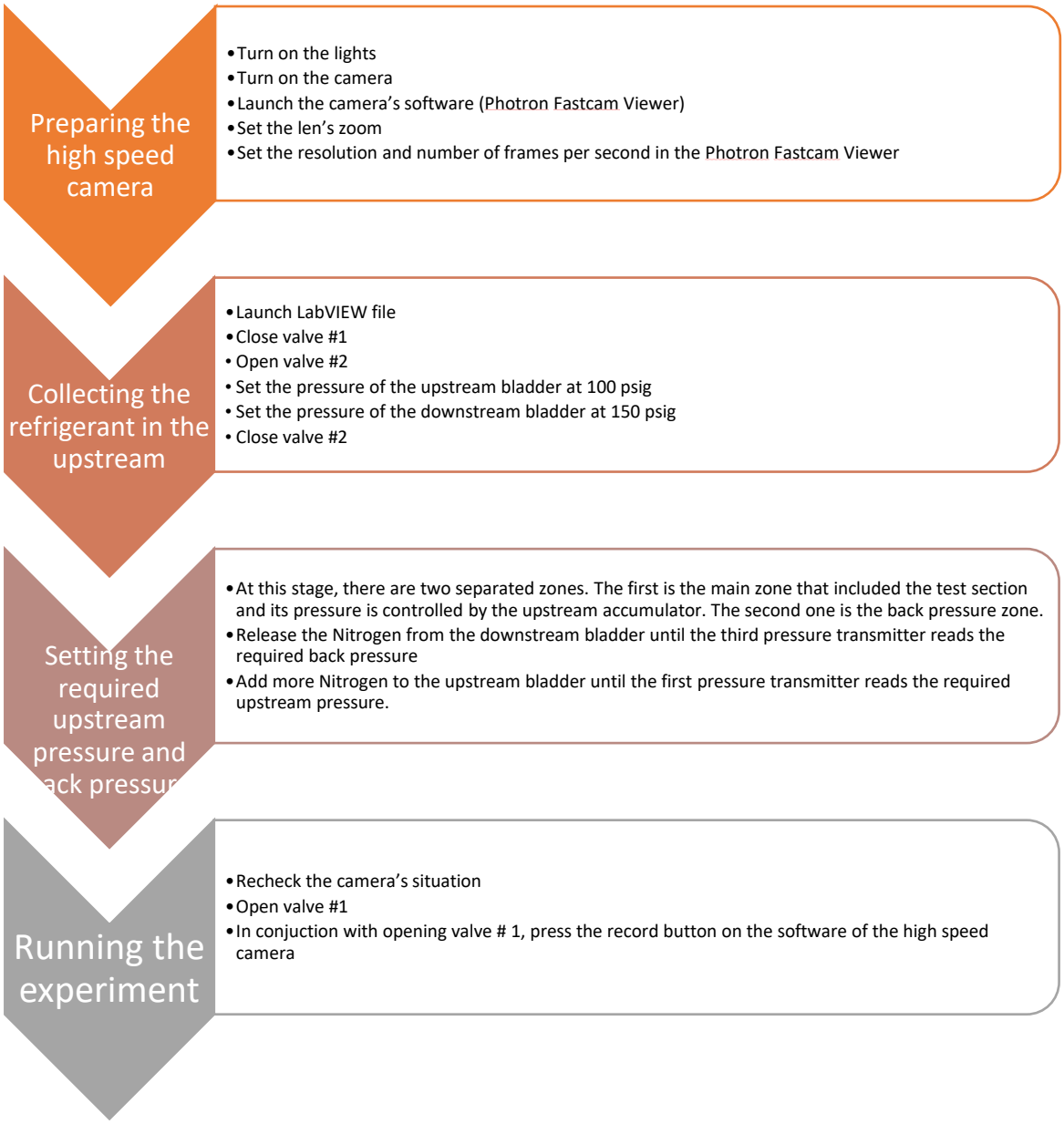

Figure 2.23 Operational procedure

Chapter 3 - Experimental Results and Analysis

This chapter will present the experimental results and provide a comparison between the two nozzles that were used in the experiments. An analysis of the results is also provided in this chapter.

3.1 Calculations of Throat Velocity and Throat Pressure

This section shows how to calculate the velocity and pressure at the throat. There were five measured values in the system: upstream pressure, downstream pressure, upstream temperature, downstream temperature, and mass flow rate. The calculated values depend on these measured values and the refrigerant properties tables. Equation 3.1 was used to estimate the throat velocity. Equation 3.2 is the Bernoulli equation that was used to estimate the throat pressure. Some assumptions which were supposed to simplify the equation of throat pressure. The assumptions are listed below:

1- $\rho_{th} = \rho_d = \rho$

2- $z_{th} = z_d$

According to these assumptions, equation 3.3 was a simplified form of equation 3.2.

$$V_{th} = \frac{m\,v}{A_t} \qquad (3.1)$$

$$\frac{P_{th}}{\rho_{th}} + \frac{V_{th}^2}{2} + z_{th}g = \frac{P_d}{\rho_d} + \frac{V_d^2}{2} + z_d g \quad (3.2)$$

$$P_{th} = P_d - \rho(\frac{V_{th}^2}{2} - \frac{V_d^2}{2}) \quad (3.3)$$

Where:

V_{th}: Throat velocity

m: Mass flow rate

v : Specific volume of liquid

A_t: Throat area

P_{th}: Throat pressure

P_d: Downstream pressure

ρ_{th}: Throat density

ρ_d: Downstream density

z_{th}: Throat elevation

z_d: Downstream pipe elevation

V_d: Downstream velocity

3.2 Experimental Results

This section presents the results of both nozzles with several starting pressure in the accumulator bladder. Each one of Figures 3.1 through 3.14 is for one run. The main difference among the runs is in the upstream pressure. Each figure contains five curves. One is for the upstream pressure, another curve is for the downstream pressure, and the third curve is for the mass flow rate. These three curves contains measured data. There is another curve for the estimated pressure at the throat, the calculation of which is explained in Section 3.1. To clarify whether the throat pressure dropped below the vapor pressure, there is a line that indicates the vapor pressure depending on the room temperature at the time of the run. Before opening valve #1, the upstream and downstream pressures were equal because the valve is after the downstream pressure transducer. The starting of the pressure drop indicated that the valve was opened and the flowing had begun. The flowing continued until the upstream pressure and downstream pressure were the same.

3.2.1 Results of nozzle #1

This section explains the results of the experiment when nozzle #1 was used. Figures 3.1 through 3.4 show the results of the runs when the upstream pressure was 200, 250, 275 and 300 psia, respectively. In the four runs, the throat pressure dropped below the vapor pressure but the cavitation didn't happen for two reasons. First, the throat pressure remained below the vapor pressure a relatively short period of time. Second, the pressure difference between the vapor pressure and minimum throat pressure was low (below 10 psi). The results show a direct relationship between the flow rate and the upstream pressure.

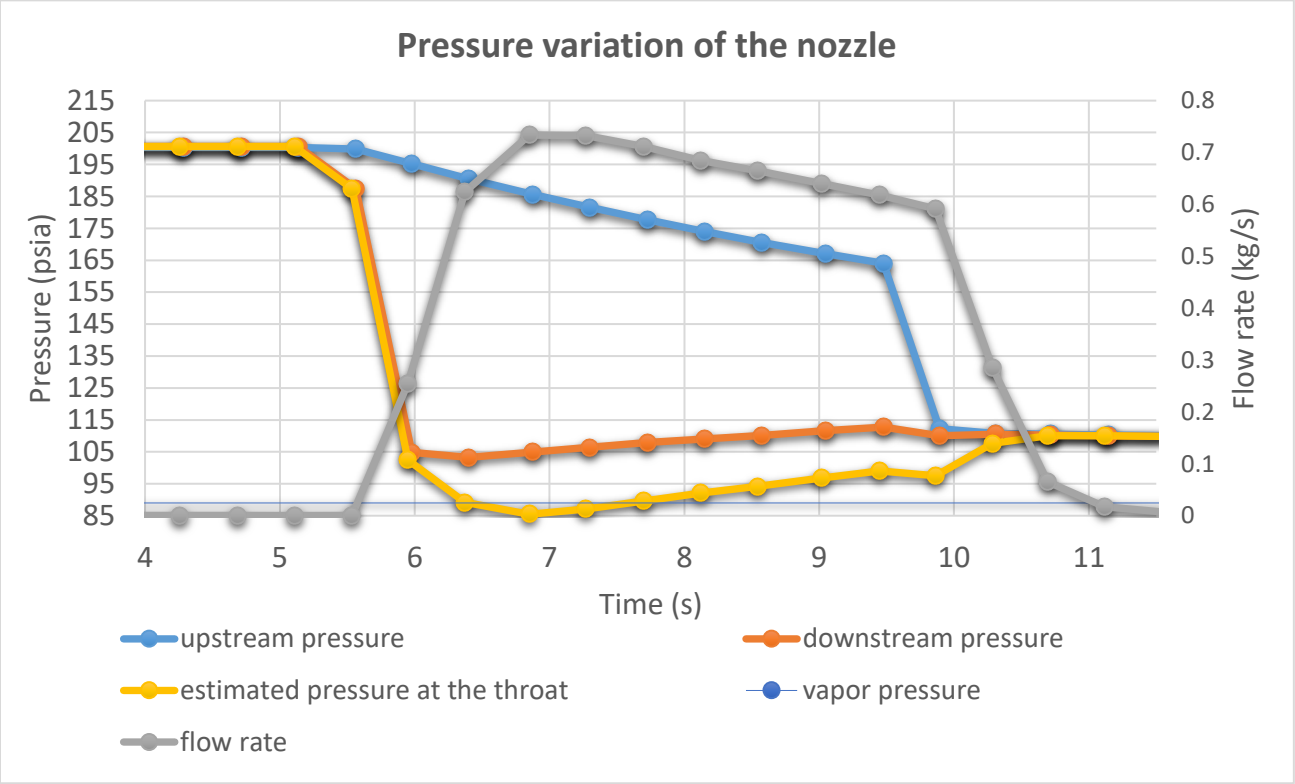

Figure 3.1 Pressure variation of nozzle #1 when the upstream pressure is 200 psia

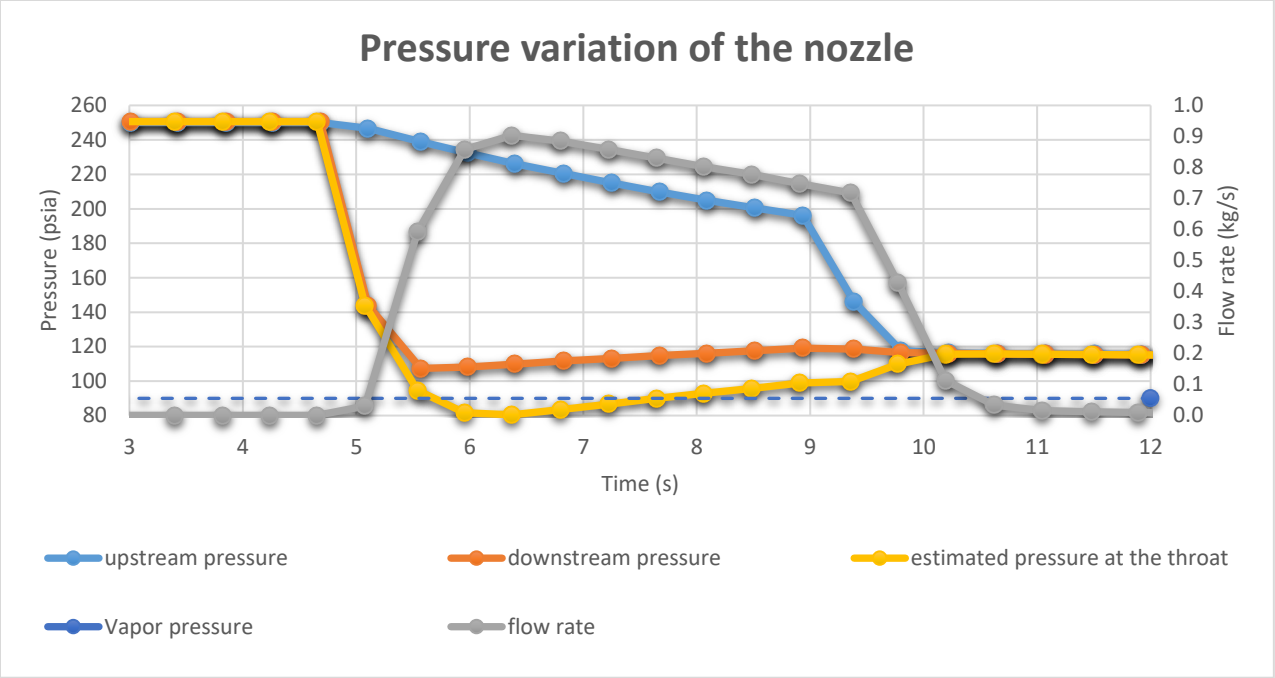

Figure 3.2 Pressure variation of nozzle #1 when the upstream pressure is 250 psia

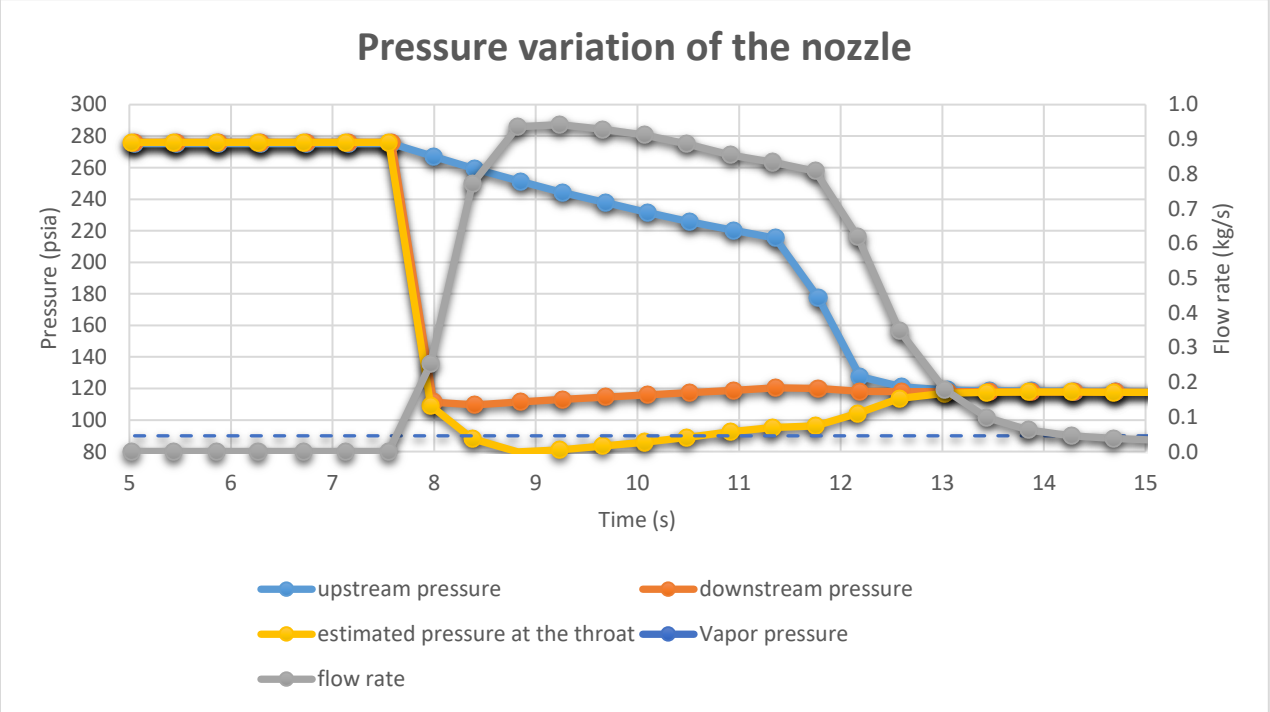

Figure 3.3 Pressure variation of nozzle #1 when the upstream pressure is 275 psia

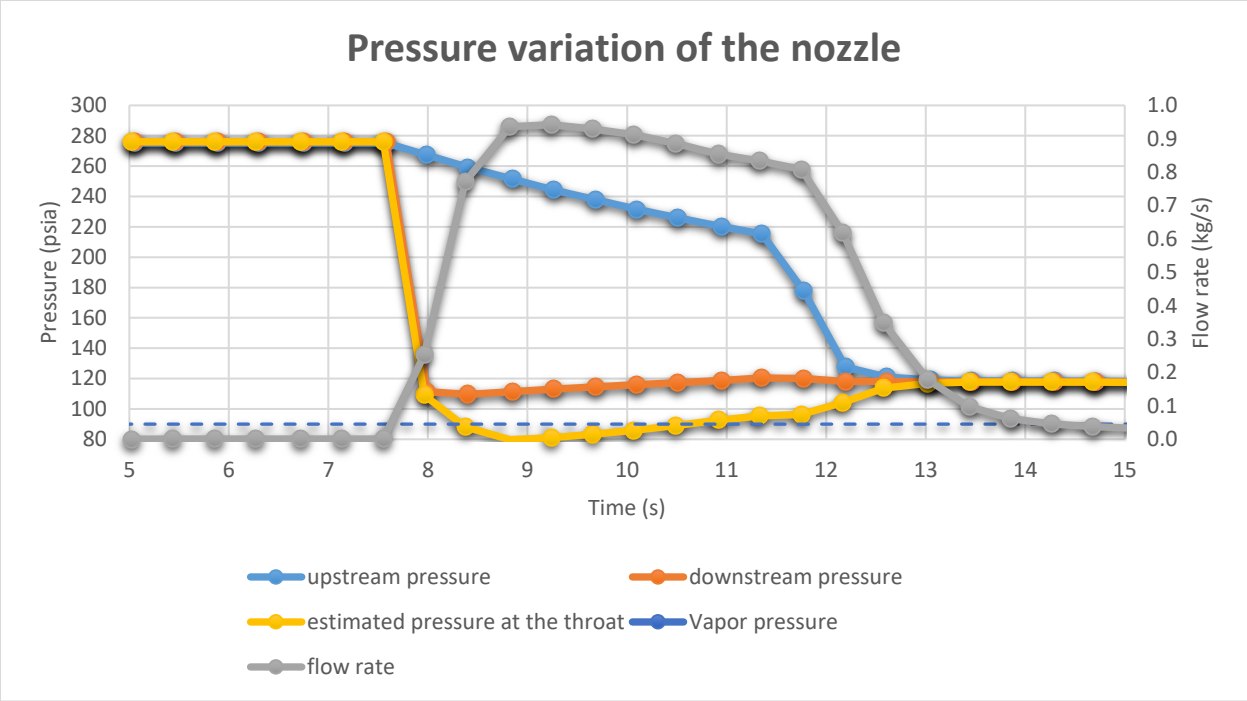

Figure 3.4 Pressure variation of nozzle #1 when the upstream pressure is 300 psia

3.2.2 Results of nozzle #2

Figures 3.5 through 3.14 show the results of nozzle #2 with upstream pressures of 200, 225, 250, 275, and 300 psia, respectively. The cavitation occurred when the upstream pressure was 200 psia or more and that was verified by the high speed camera. In these runs, the throat pressure was below the vapor pressure for two or more seconds. The difference between the vapor pressure and the lowest throat pressure was 15 psi when the upstream pressure was 200 psia; it was 26 psi when the upstream pressure was 300 psia.

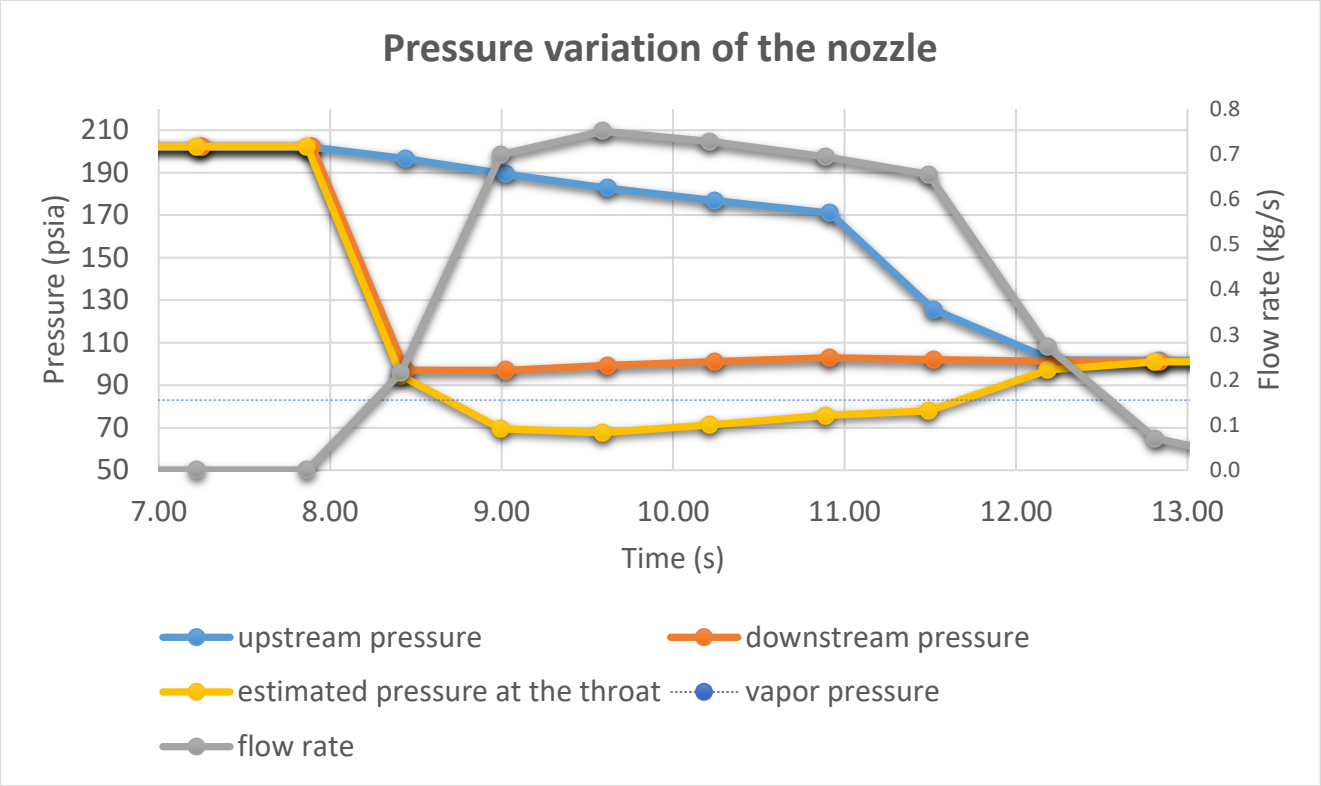

Figure 3.5 Pressure variation of nozzle #2 when the upstream pressure is 200 psia

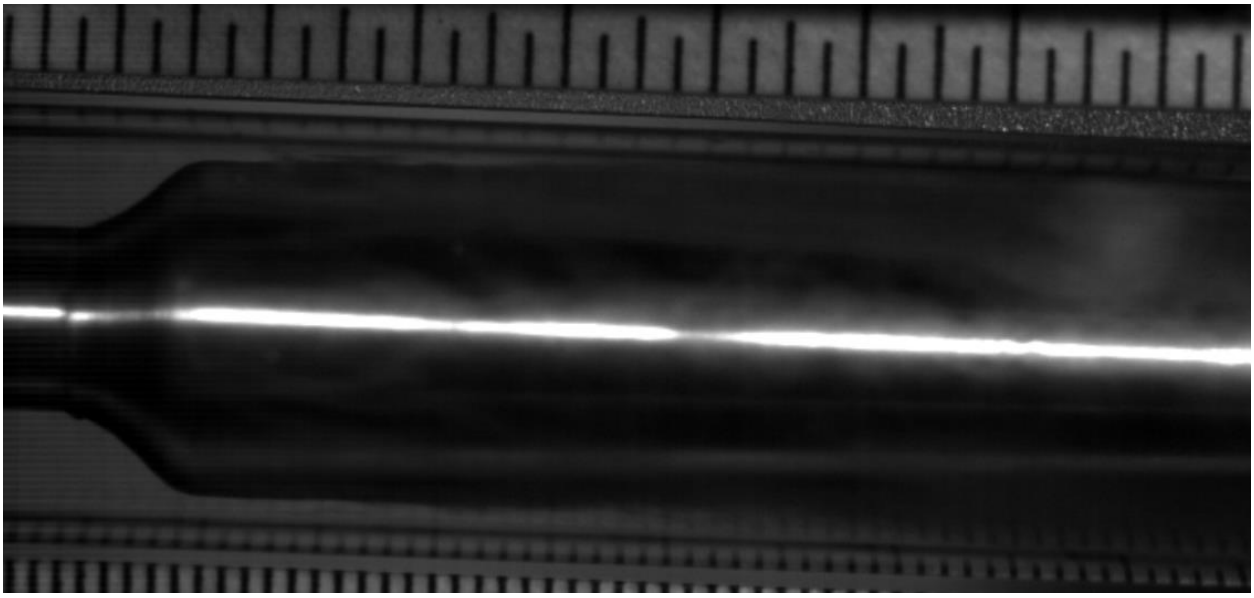

Figure 3.6 Screen shot of the video from high-speed camera when the upstream pressure is 200 psia

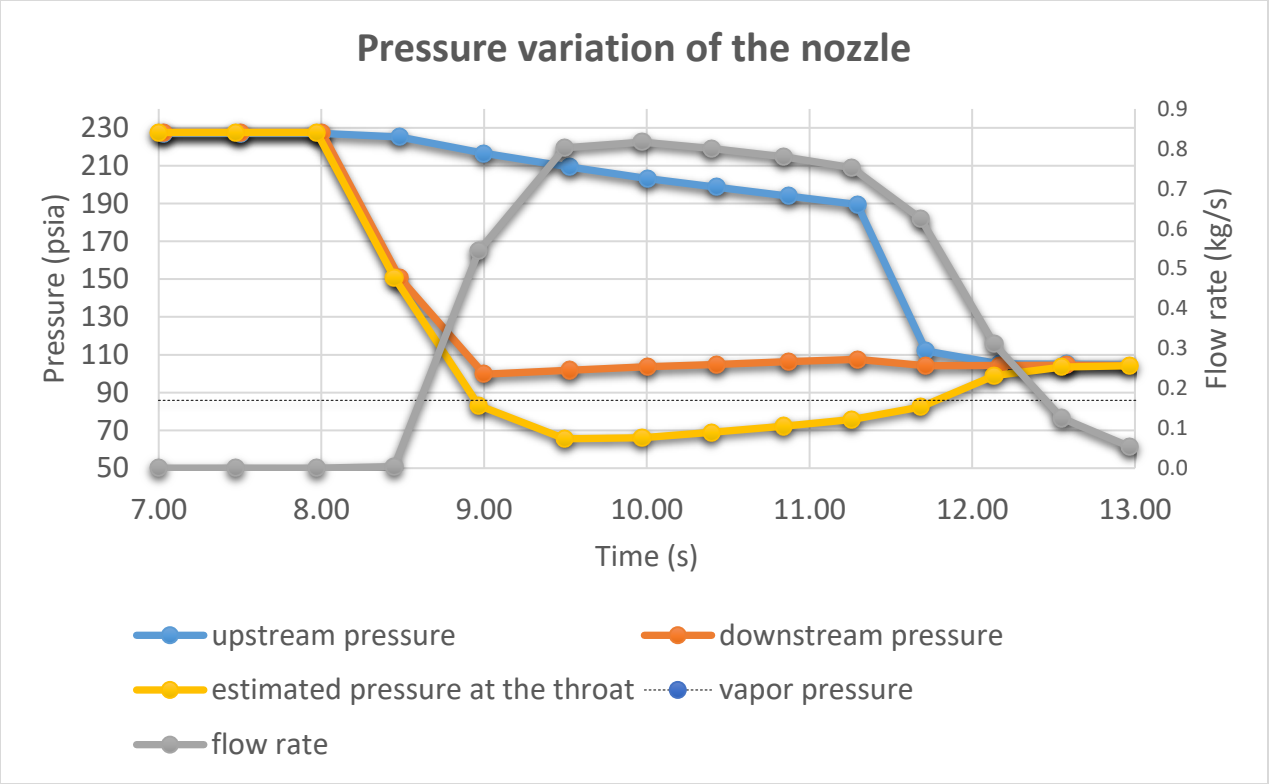

Figure 3.7 Pressure variation of nozzle #2 when the upstream pressure is 225 psia

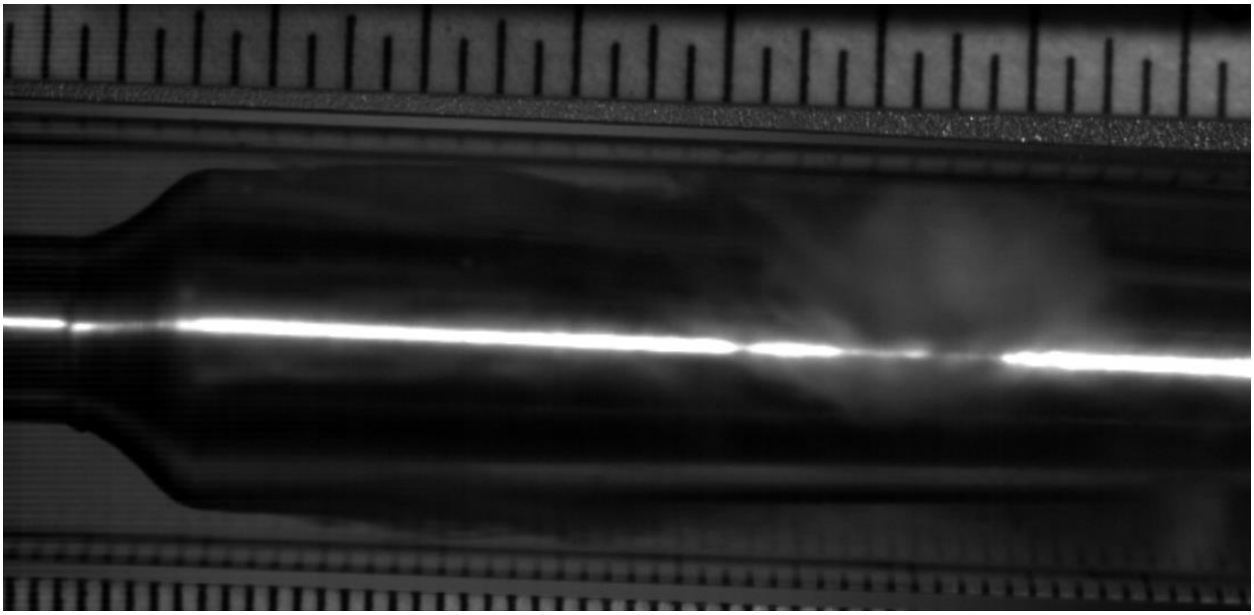

Figure 3.8 Screen shot of the video from high-speed camera when the upstream pressure is 225 psia

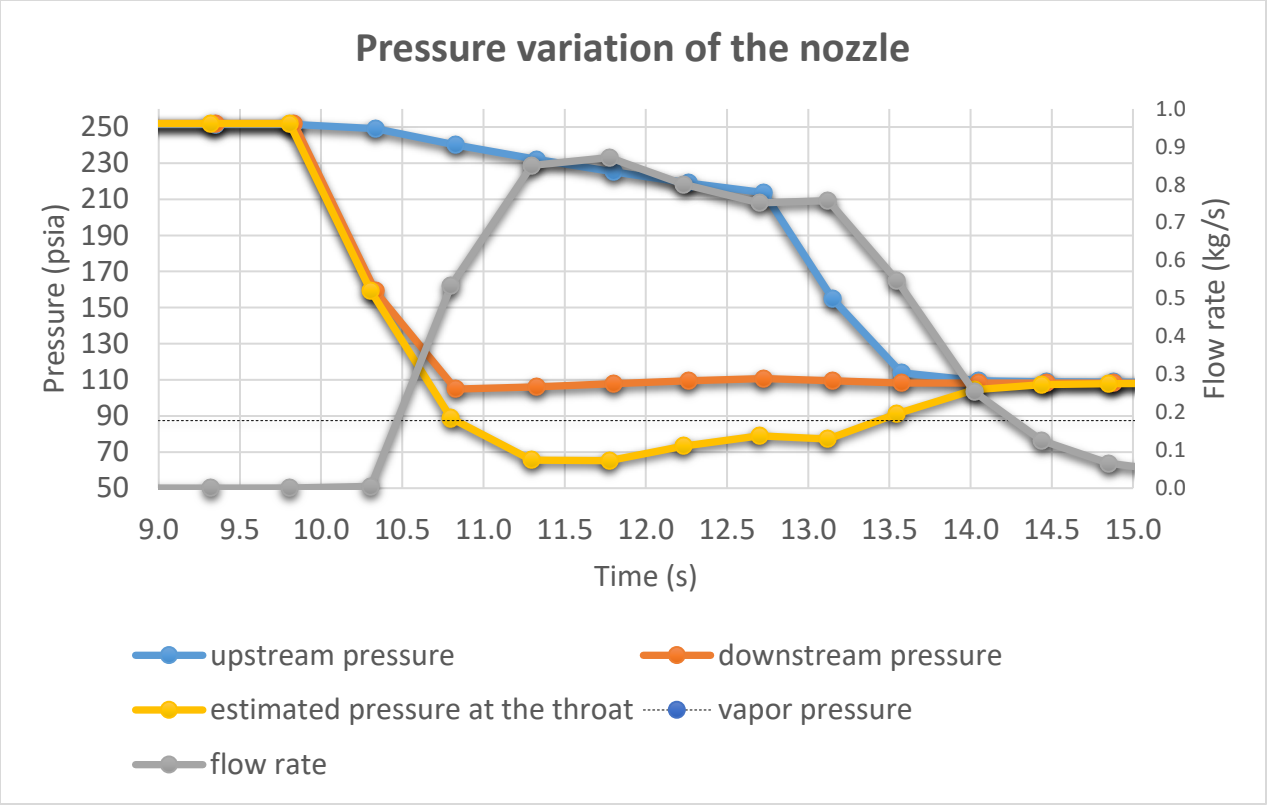

Figure 3.9 Pressure variation of nozzle #2 when the upstream pressure is 250 psia

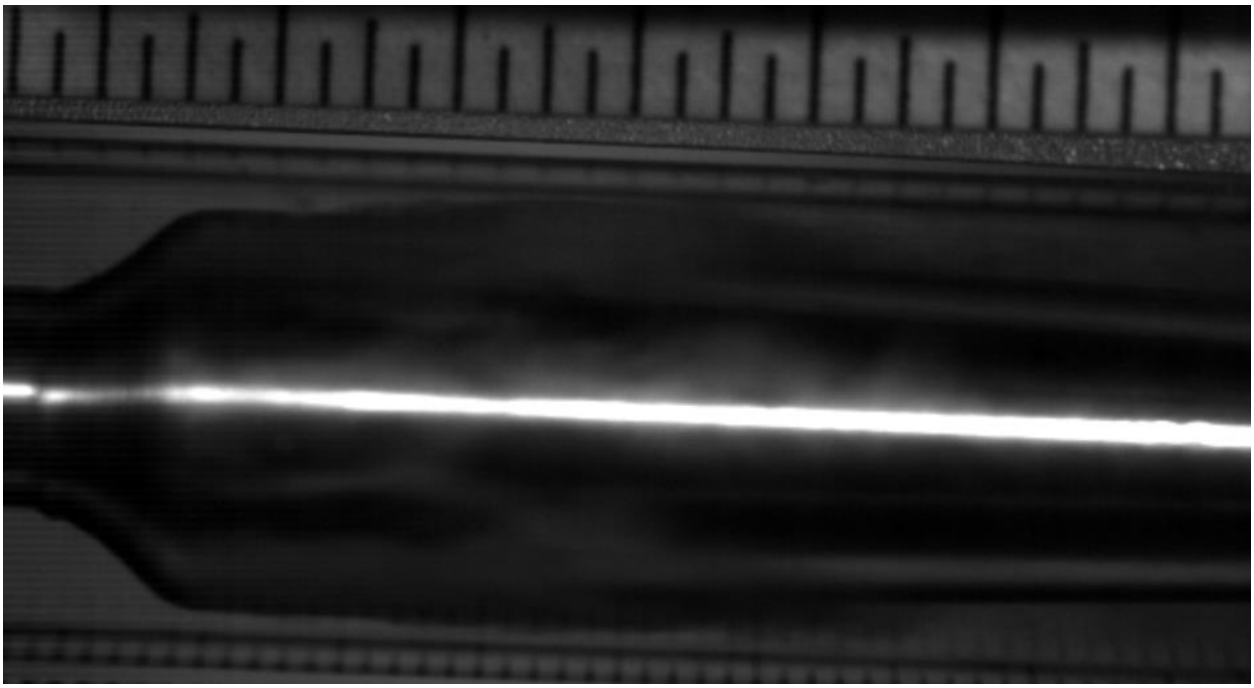

Figure 3.10 Screen shot of the video from high-speed camera when the upstream pressure is 250 psia

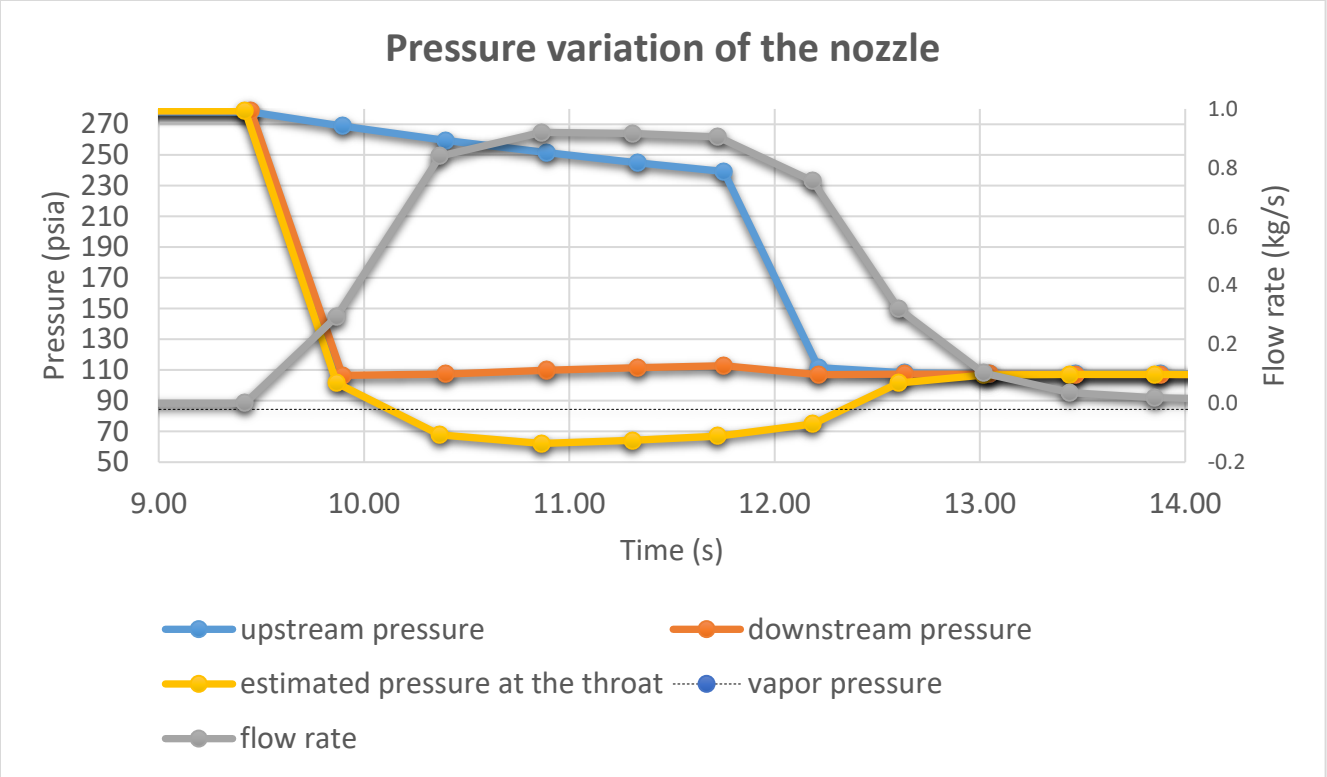

Figure 3.11 Pressure variation of nozzle #2 when the upstream pressure is 275 psia

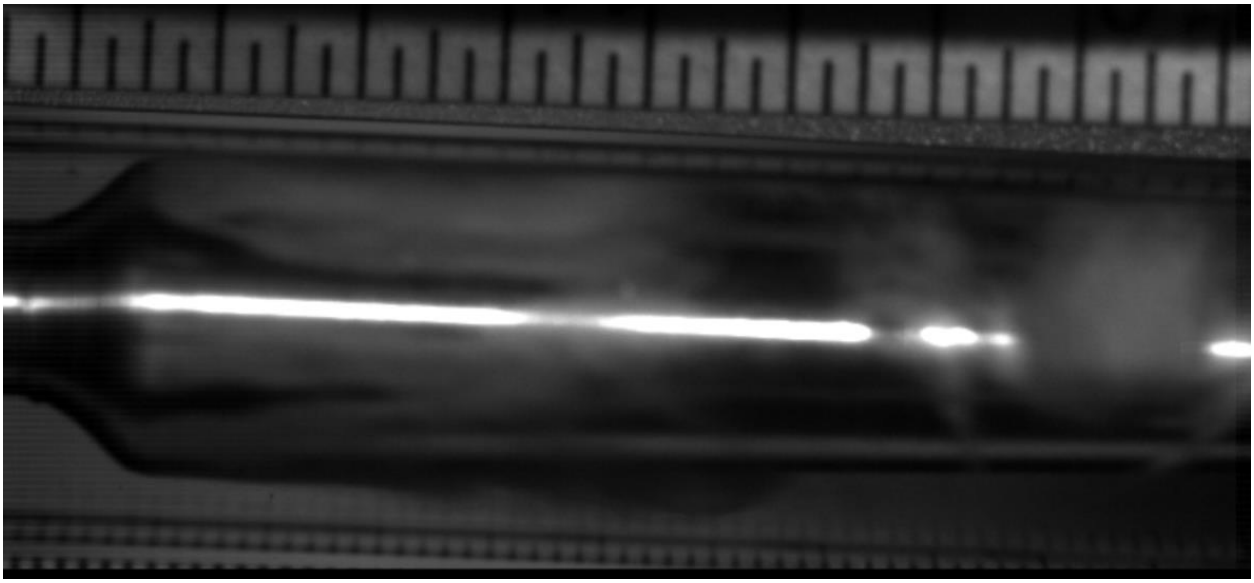

Figure 3.12 Screen shot of the video from high-speed camera when the upstream pressure is 275 psia

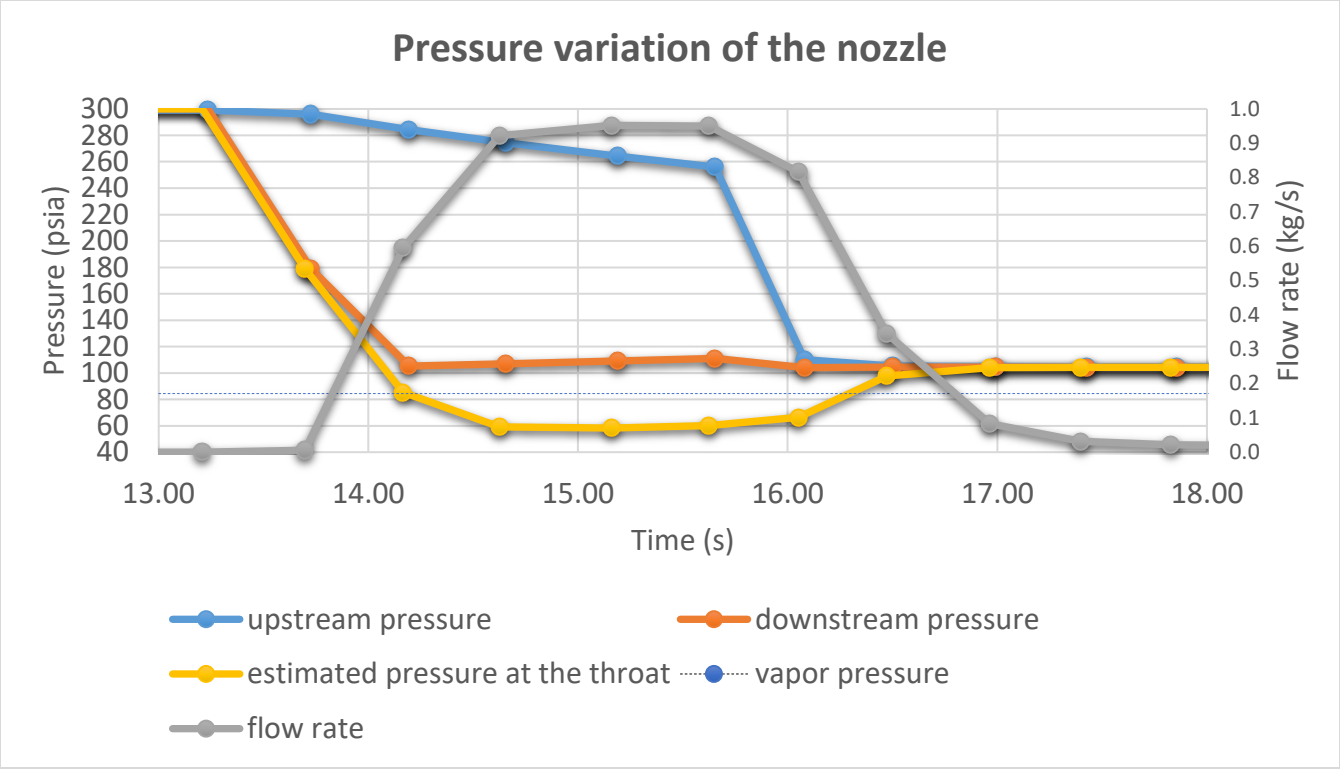

Figure 3.13 Pressure variation of nozzle #2 when the upstream pressure is 300 psia

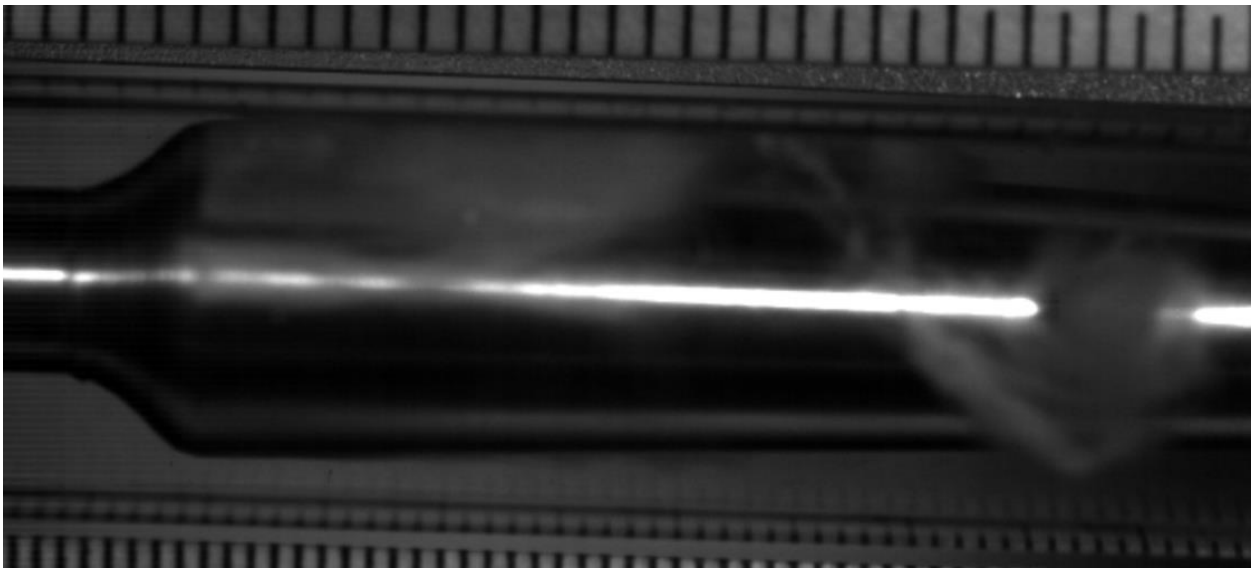

Figure 3.14 Screen shot of the video from high-speed camera when the upstream pressure is 300 psia

3.3 Turbulent Flow

Deciding whether the flow was laminar or turbulent, required calculation of the Reynolds number. For the internal flow flow, the flow was turbulent if the Reynolds number was more than 2300, and the flow is laminar if the Reynolds number is less than 2300. Equation 3.4 shows the Reynolds number.

$$Re = \frac{\rho V D_h}{\mu} \qquad (3.4)$$

$$D_h = Inner\ tube\ diameter - insert\ diameter \qquad (3.5)$$

Where:

ρ: Density

D_h: Hydraulic diameter

μ: Dynamic viscosity

V: $velocity$

The results express that the flow is always turbulent whether it is cavitating or not. Figure 3.15 shows the results of nozzle #1 with upstream pressure at 200 psia while Figure 13.16 shows the results of nozzle #2 with upstream pressure at 300 psia. The minor vertical axis is for the Reynolds number. It is clear that the Reynolds number was much higher than 2300, which means that the flow was likely turbulent.

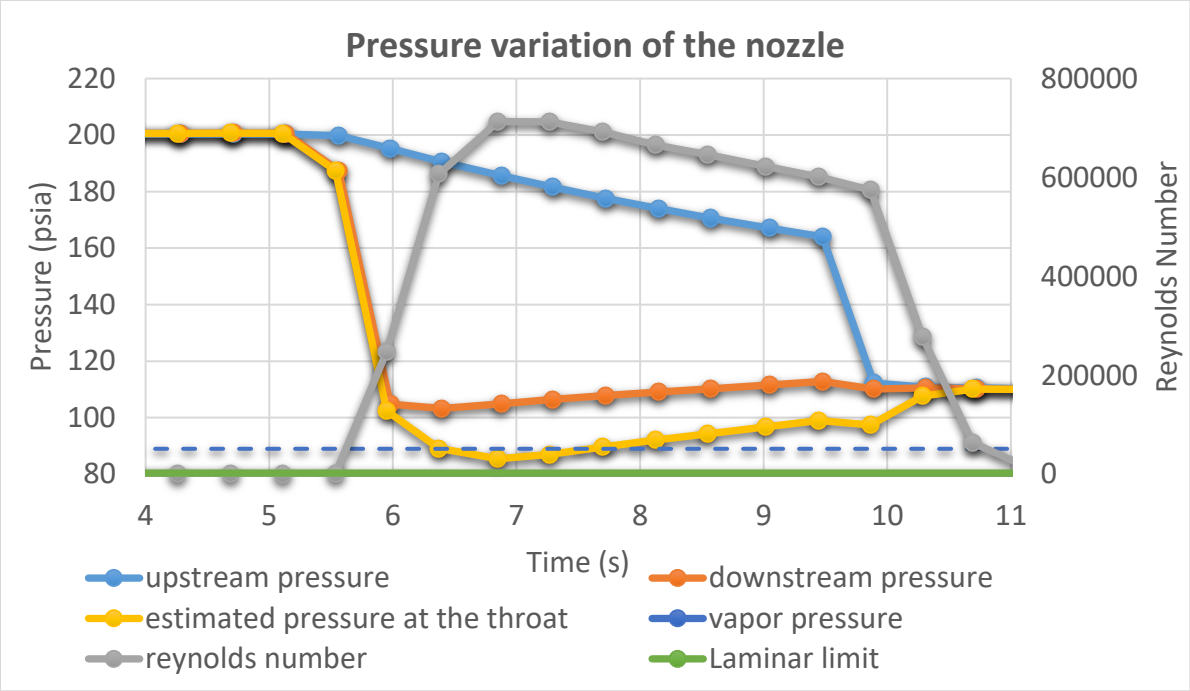

Figure 3.15 Pressure variation of nozzle #1 when the upstream pressure is 200 psia with Reynolds number

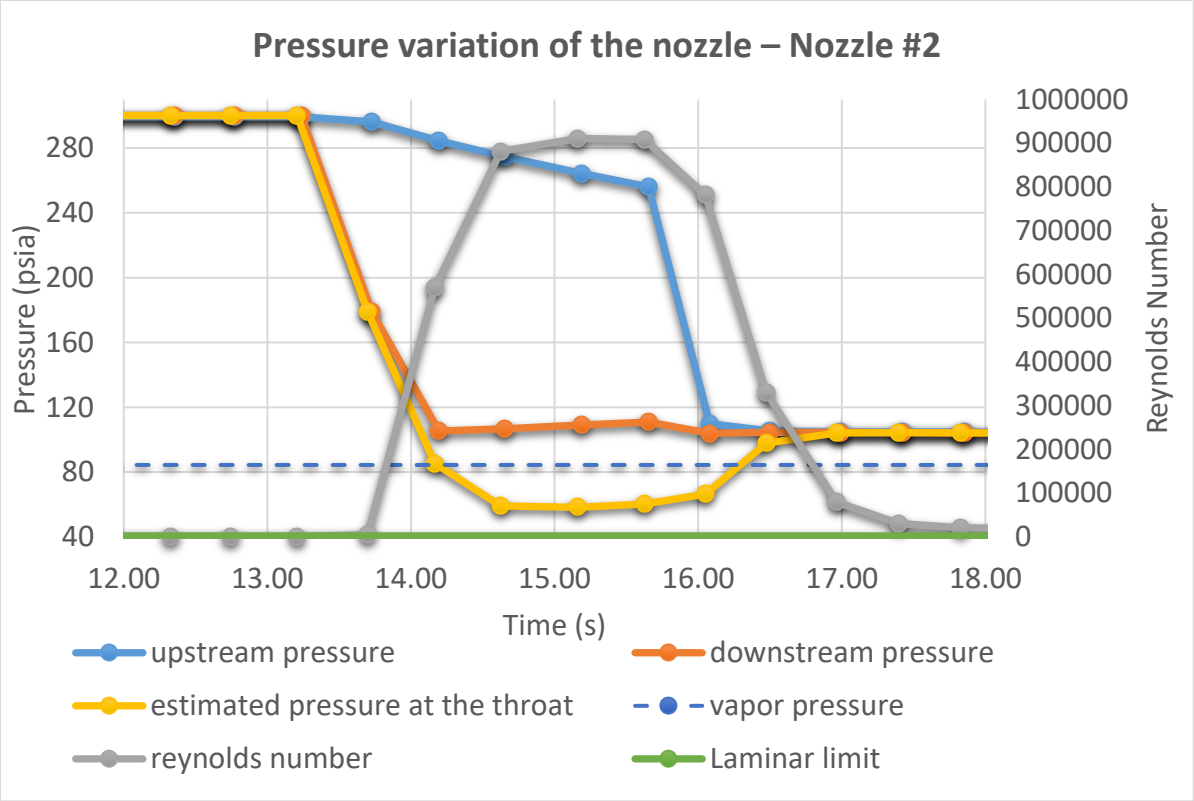

Figure 3.16 Pressure variation of nozzle #2 when the upstream pressure is 300 psia with Reynolds number

3.4 Cavitation Initiation

According to the videos, the cavitation initiation was exactly at the throat. Figure 3.17 contains several shots for different upstream pressures. It is clear that in all of them, the cavitation onset was at the throat. Also from the video, the investigator observed that the nucleation in the test section was heterogeneous because it was created at the contact surface of the fluid and the insert. As mentioned in Chapter One, there are four types of cavitation: traveling bubble cavitation, vortex cavitation, sheet/cloud cavitation, and attached cavitation. The video shows that the achieved cavitation was attached cavitation. Figure 3.18 tracks the nucleation at a certain spot from the cavitation onset when that spot was activated as a nucleation site to the end.

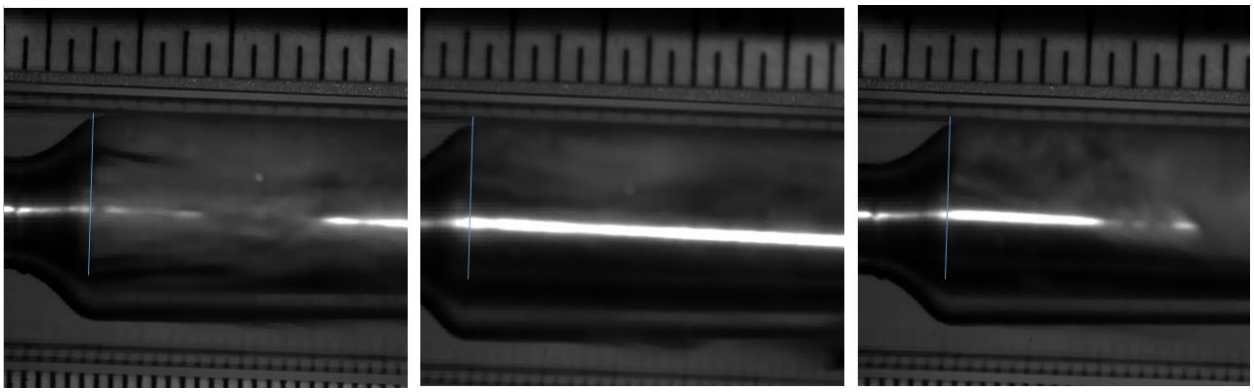

Figure 3.17 Cavitation initiation at the throat

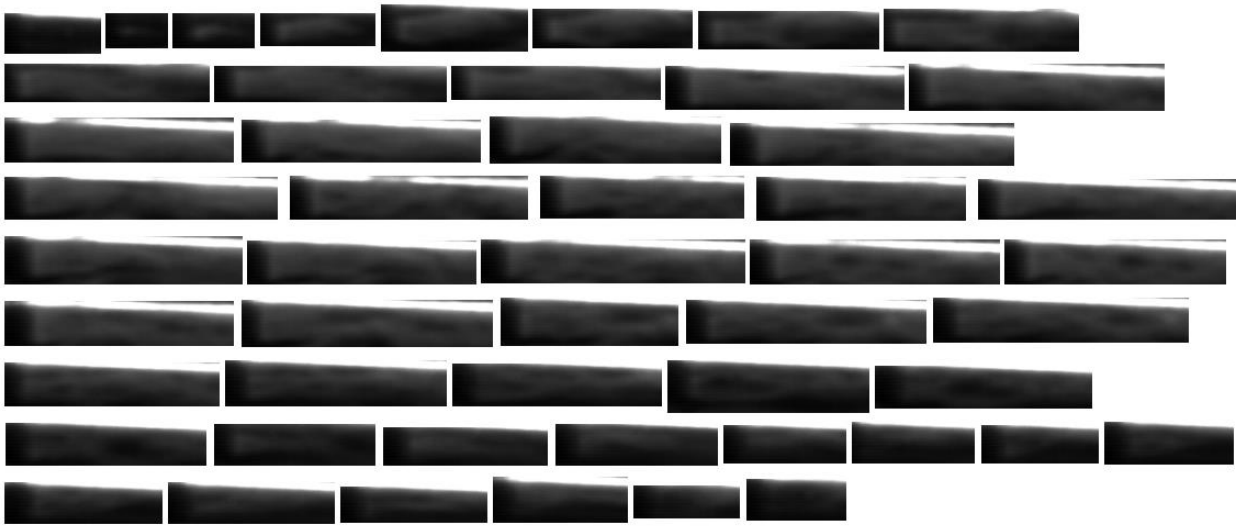

Figure 3.18 Tracking of cavitation onset for a certain spot

3.5 The Relation Between Vibration and The Upstream Pressure

One of the observations from the recorded videos was that there was vibration caused by the cavitation. There are two questions that need to be answered: Is the vibration amplitude related to the upstream pressure? And does the vibration affect the activation of nucleation sites? The vibration amplitude had a direct relation to upstream pressure. The periodic behavior of the cavitation is more obvious with the high upstream pressure because the gap size between the insert and the glass tube was changing along the time. With relative low pressure (200 psia), the nucleation was stable because the vibration amplitude was small.

The nucleation sites were not activated during the run, but each one was active for a certain time if the gap decreased or inactive if the gap increased. From the videos, a particular spot was selected for investigation. For each upstream pressure, the time that the spot was active was computed and that was repeated five times. The results are shown in Figure 3.19. As the figure indicates, the spot remained as an active nucleation site for longer with lower upstream pressure. When the upstream pressure was 200 psia, there was a vibration but with relatively low amplitude.

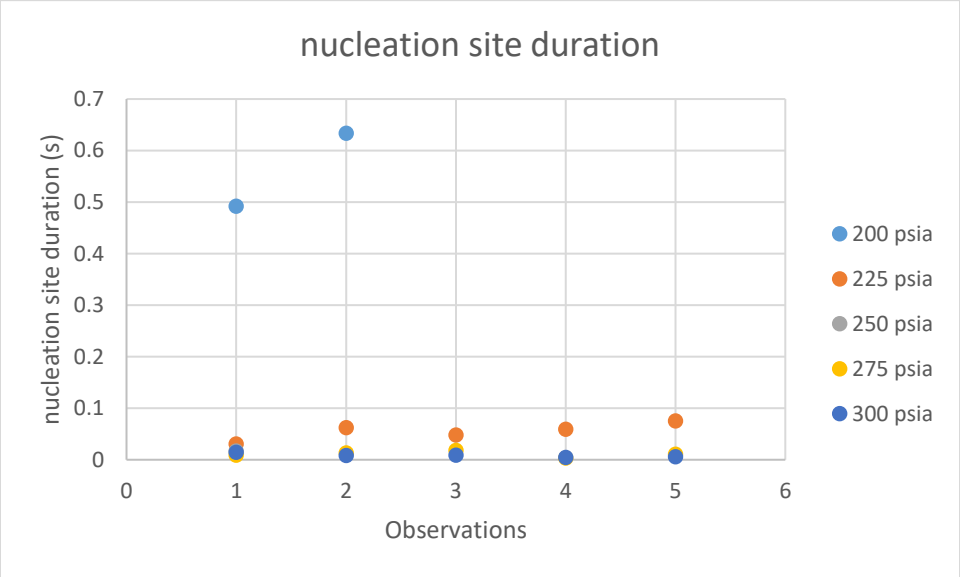

Figure 3.19 Nucleation site duration

3.6 Cavitation Number and Coefficient of Pressure

As mentioned in Chapter 1, the comparison of the cavitation number with negative coefficient of pressure can predict whether cavitation is possible. If the cavitation number is less than negative coefficient of pressure (–Cp), the fluid is in the metastable zone. On the other hand, if the cavitation number is more than the negative coefficient of pressure, there will be no cavitation at all. Figures 3.20 through 3.23 show the comparison of the cavitation number and the negative of the coefficient of pressure at the lowest pressure points. Figure 3.20 is for nozzle

#1 when the upstream pressure is 200 psia while Figure 3.21 is also for nozzle #1 but with an upstream pressure of 300 psia. Figures 3.22 and 3.23 are for nozzle #2 and the difference between them is that Figure 3.22 is for upstream pressure 200 psia and Figure 3.23 is for upstream pressure 300 psia. In Figures 3.20 and 3.21, the cavitation number is more than –Cp, so there is no cavitation. As shown in Figures 3.22 and 3.23, cavitation occurred with nozzle #2 because the cavitation number was less than –Cp. The charts in figures 3.20 through 3.23 confirmed the credibility of using cavitation number and –Cp to predict the possibility of the cavitation because the charts' date matched the experimental results.

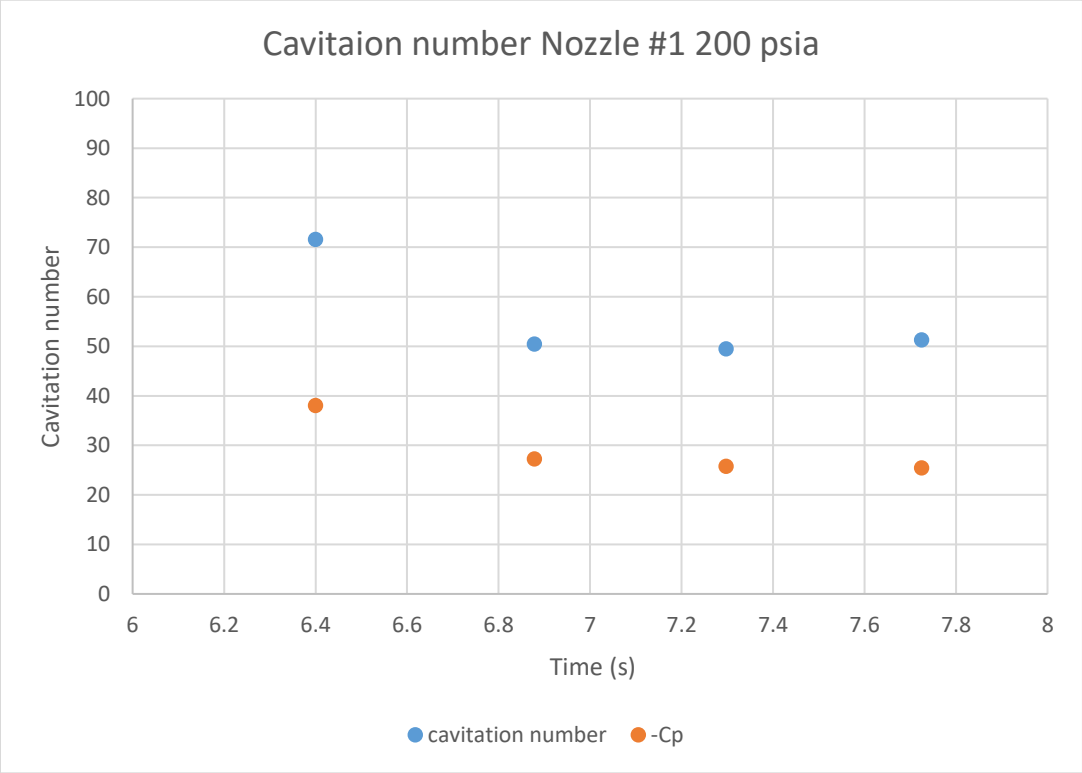

Figure 3.20 Relation between cavitation number and –Cp for nozzle #1 when the upstream pressure is 200 psia

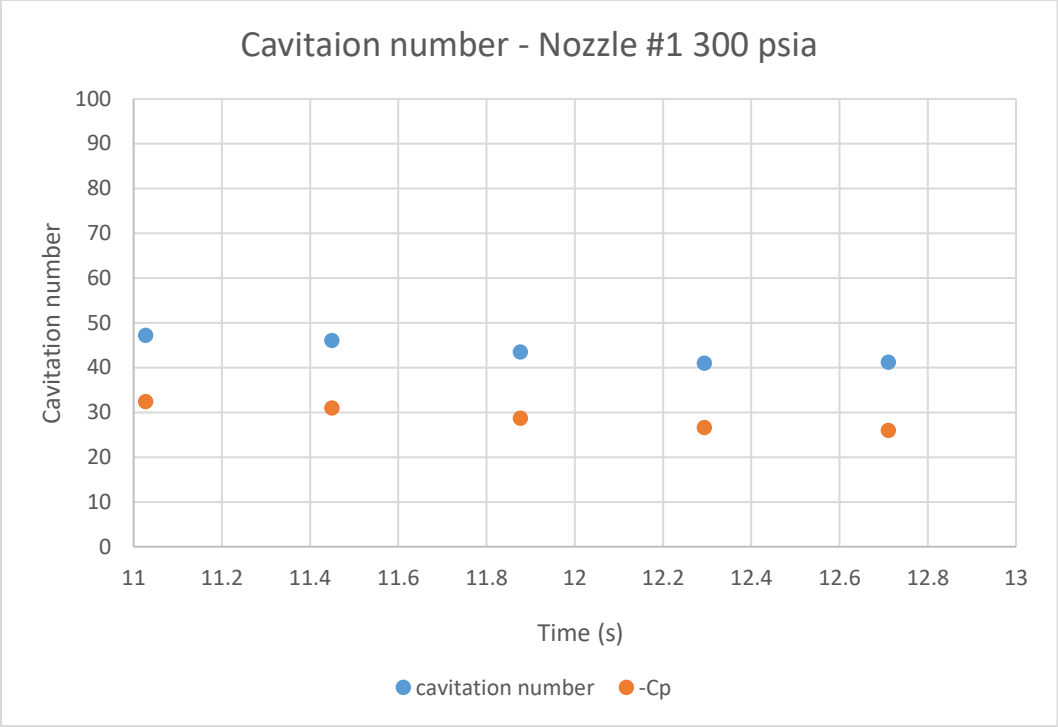

Figure 3.21 Relation between cavitation number and –Cp for nozzle #1 when the upstream pressure is 300 psia

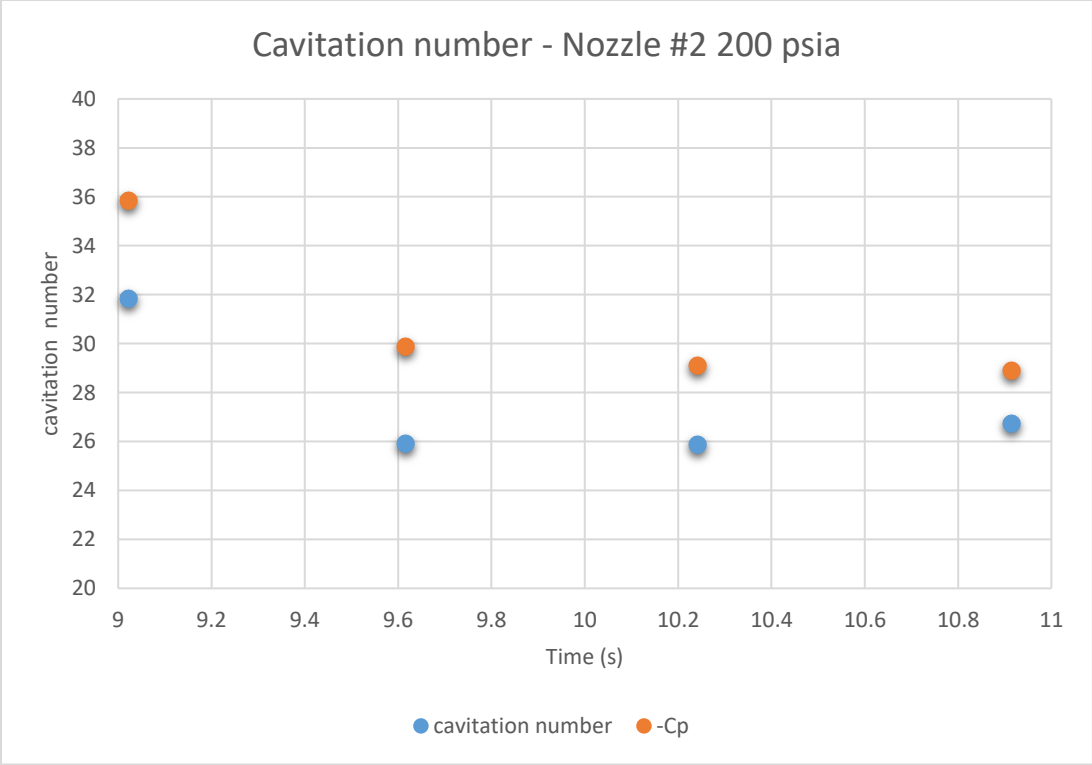

Figure 3.22 Relation between cavitation number and –Cp for nozzle #2 when the upstream pressure is 200 psia.

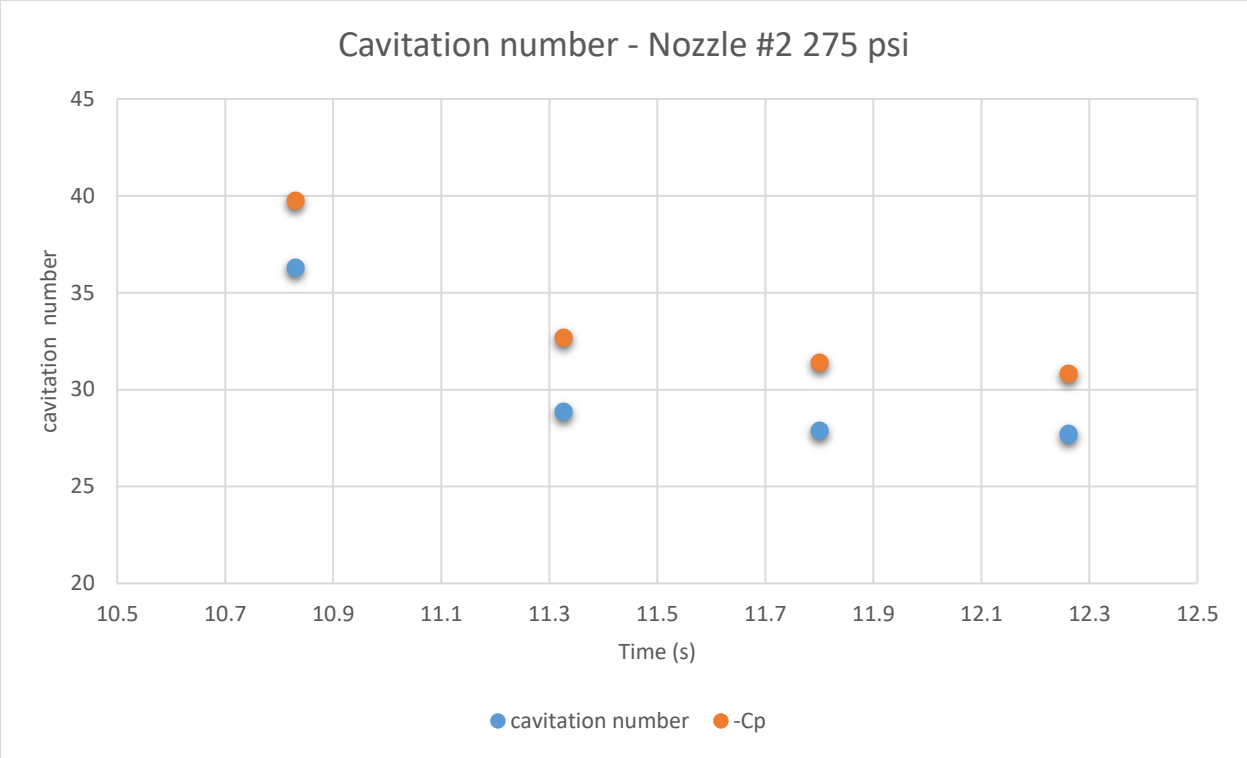

Figure 3.23 Relation between cavitation number and –Cp for nozzle #2 when the upstream pressure is 275 psia.

3.7 The Impact of Minimizing The Gap at The Throat

The uniqe difference between the two tested nozzles is in the gap at the throat. The gap of nozzle #1 is 1 mm while it is 0.8 mm in nozzle #2. Figure 3.24 and Figure 3.25 present the relationship between the velocity at the throat and the difference between vapor pressure and throat pressure.

The throat velocity had a direct relation to the upstream pressure and an inverse relation to the gap. The figures below demonstrate that minimization of the gap gave more pressure drop below the vapor pressure which meant a higher degree of metastability.

The results show that cavitation didn't occur when the pressure drop (vapor pressure - throat pressure) was less than 10 psi, and that was what was observed with nozzle #1. When the

pressure drop was 14 psi or more, cavitation occured, and that was what was observed with nozzle #2.

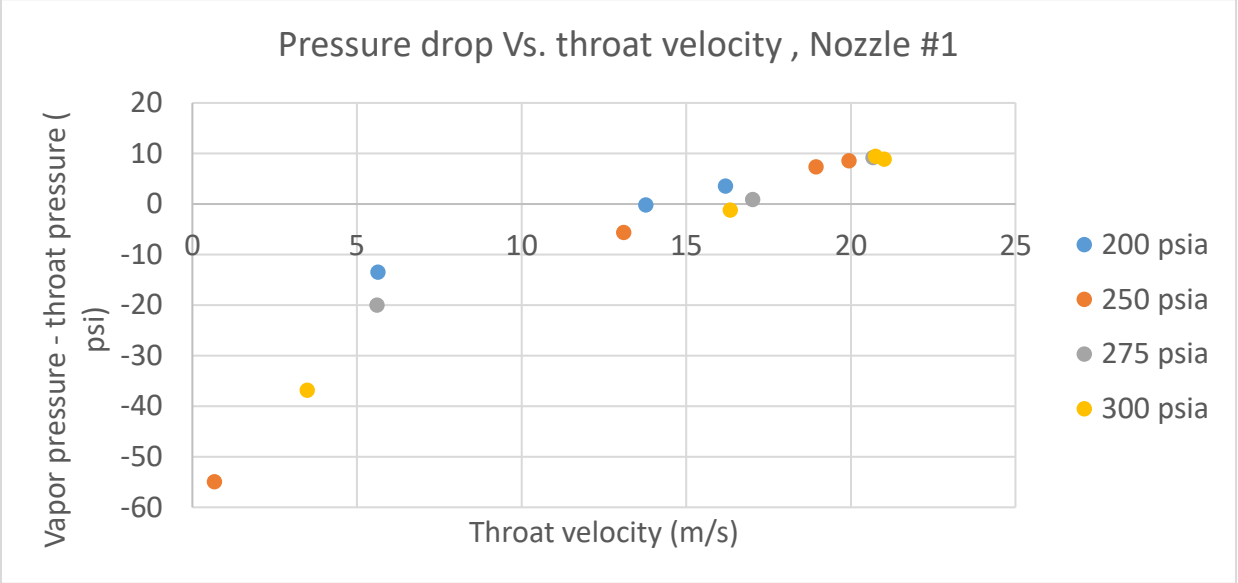

Figure 3.24 Pressure drop vs. throat velocity of nozzle #1

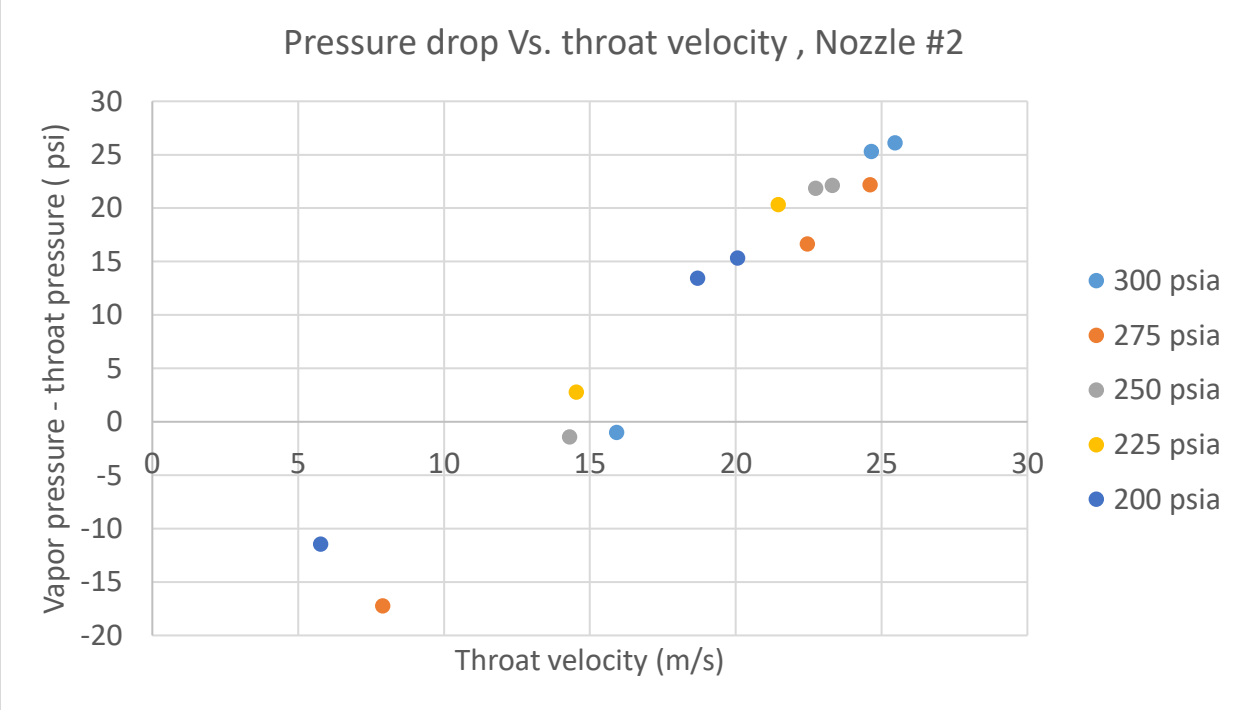

Figure 3.25 Pressure drop vs. throat velocity of nozzle #2

3.8 The Loss Coefficient

The K factor is commonly used to quantify the pressure drop through orifice flow meters. In this case, it was insightful to analyze this system as a single $\acute{K}$ factor. The factor included the major losses and minor losses. The factor was calculated with several upstream pressures and the corresponding flow rates. The aim of the investigation was to compare the loss coefficient when the fluid was single-phase flow (liquid) with that for it was two-phase flow (liquid and vapor). Equation 3.6 is the general equation of the total head loss. The first term in the right hand side is for the major losses, while the second term is for the minor losses. By assuming ($V_1 = V_2 \; and \; z_1 = z_1$), equation 3.7 is the head loss equation according to these assumptions. The acceleration of gravity (g) was eliminated from each term in Equation 3.8. Equation 3.10 shows the K factor is for the major and minor losses. Equation 3.14 states how the $\acute{K}$ factor was calculated in the analyzed cases.

$$\left(\frac{P_1}{g\rho_2} + \frac{V_1^2}{2g} + z_1\right) - \left(\frac{P_2}{g\rho_2} + \frac{V_2^2}{2g} + z_1\right) = f\frac{L}{D}\frac{V^2}{2g} + \Sigma k\frac{V^2}{2g} \tag{3.6}$$

$$\frac{P_1 - P_2}{\rho g} = f\frac{L}{D}\frac{V^2}{2g} + \Sigma k\frac{V^2}{2g} \tag{3.7}$$

$$\frac{\Delta P}{\rho} = f\frac{L}{D}\frac{V^2}{2} + \Sigma k\frac{V^2}{2} \tag{3.8}$$

$$\frac{\Delta P}{\rho} = \left(f\frac{L}{D} + \Sigma k\right)\frac{V_{th}^2}{2} \tag{3.9}$$

$$\acute{K} = f\frac{L}{D} + \Sigma k \tag{3.10}$$

$$\frac{\Delta P}{\rho} = \acute{K}\frac{V_{th}^2}{2} \tag{3.11}$$

$$\acute{K} = \frac{2\Delta P}{\rho V_{th}^2} \tag{3.12}$$

$$\Delta P = P_{up} - P_d \tag{3.13}$$

$$\acute{K} = \frac{2(P_{up} - P_d)}{\rho V_{th}^2} \tag{3.14}$$

Where:

K: General loss coefficient that includes the major losses and minor losses

k : Loss coefficient of the minor losses for each part of the system

f: Friction factor

P_{up} : Upstream pressure

P_d: Downstream pressure

ρ: Density

V_{th}: Throat velocity

Figure 3.26 shows that the loss coefficient was almost constant when cavitation occurred; however, it was not constant with one-phase flow. Figure 3.26 shows the results of the loss coefficient of the two-phase flow, while Figure 3.27 shows the loss coefficient for single phase and two-phase flows.

The loss coefficient of one-phase flow was expected be less than the loss coefficient of two-phase flow but the results do not demonstrate that. One possible reason is that the pressure data and flow rate data were not synchronized well enough.

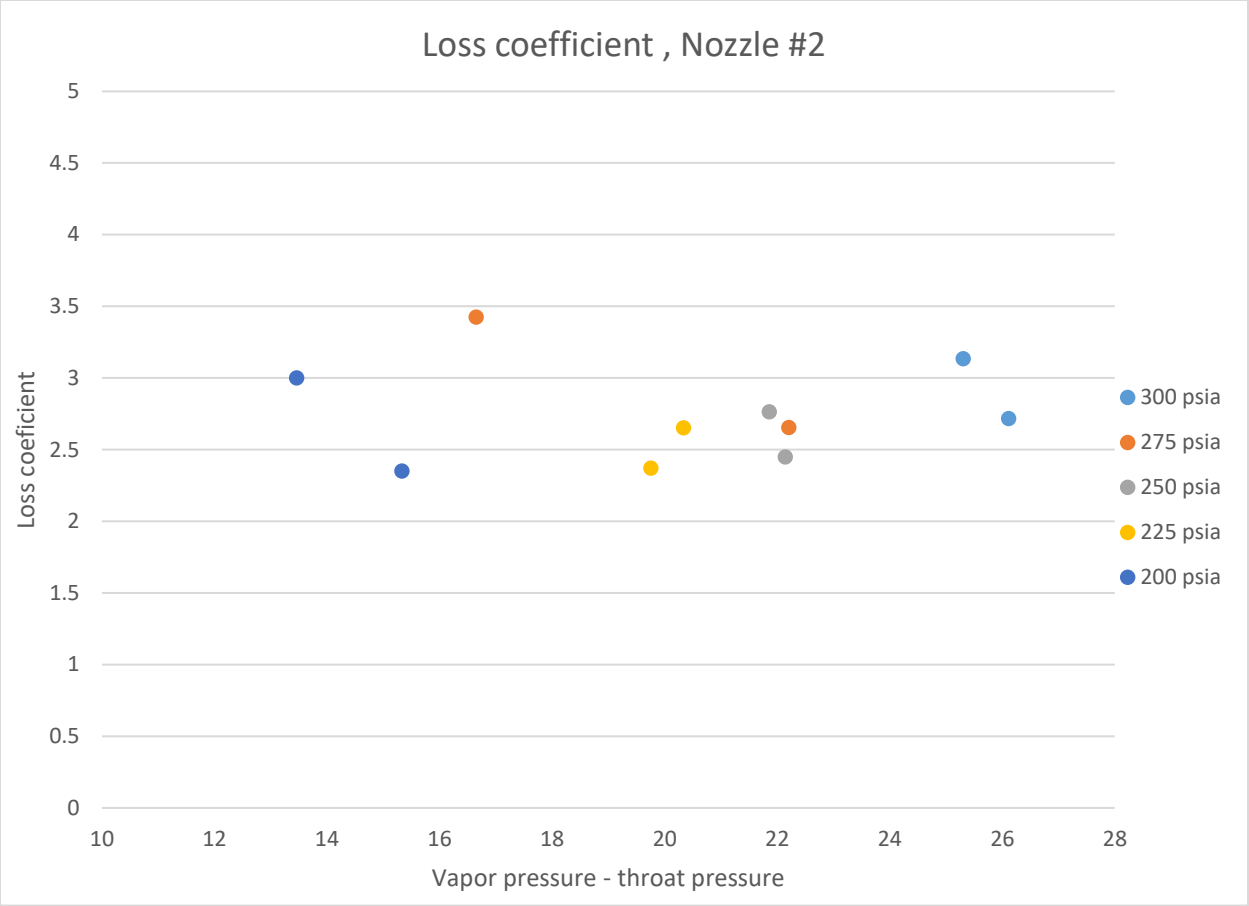

Figure 3.26 Loss coefficient for two-phase flow

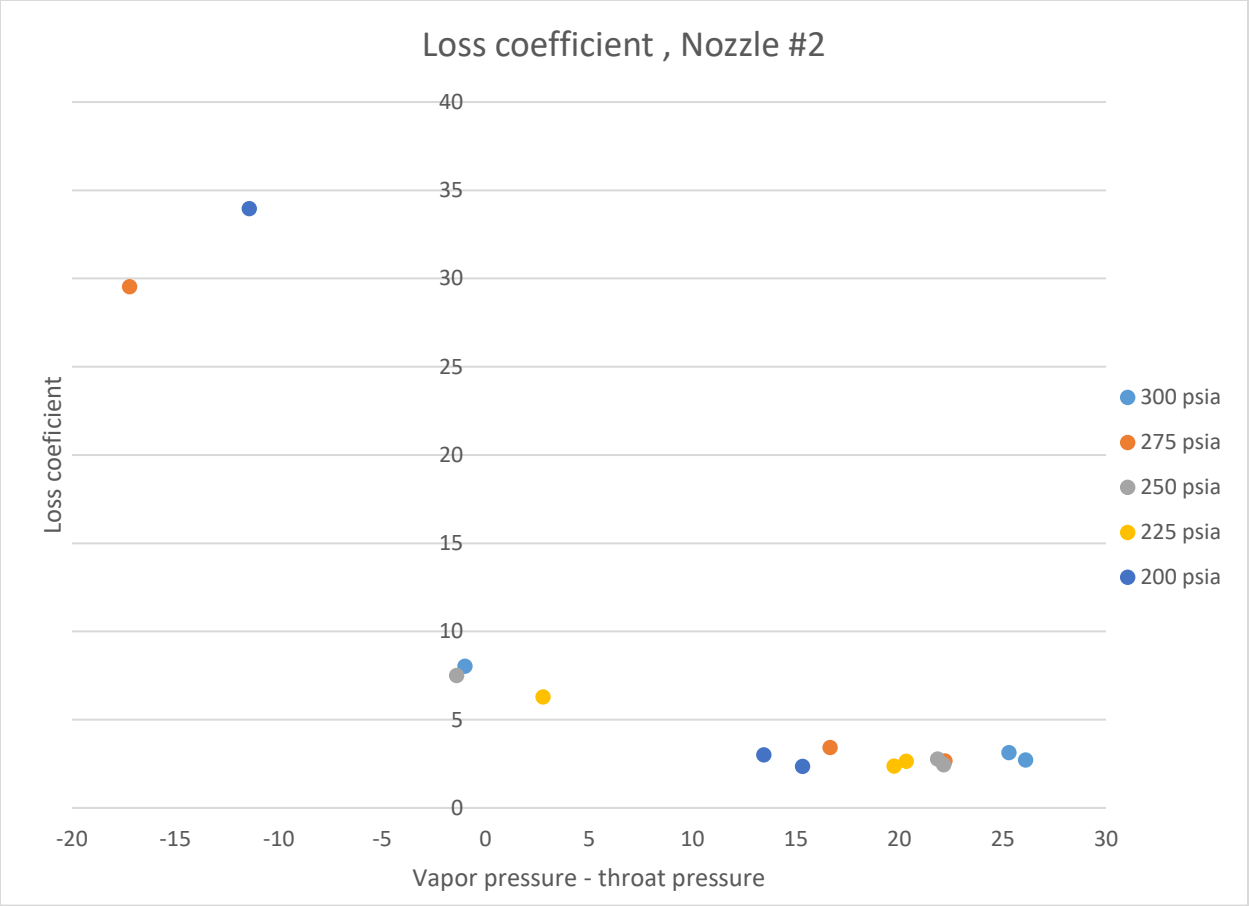

Figure 3.27 Comparison of loss coefficient with one-phase flow and with two-phase flow

Chapter 4 - Conclusion and Recommendations

4.1 Summary and Conclusion

This thesis presented the results and analysis of R134a cavitation when the refrigerant flows through a converging-diverging nozzle. Two nozzles were tested with the only difference between them being in the throat area. Decreasing the throat area enhanced the cavitation potential. The nozzle design respected transparency, sealing, compatibility with R134a, compatibility with high pressure and manufacturing simplicity. Depending on the measured values of pressure, temperature, and flowrate, throat velocity and throat pressure were calculated.

To analyze the results, several dimensionless numbers were calculated: Reynolds number, cavitation number, coefficient of pressure, and loss coefficient. According to the Reynolds number calculations, the flow was always turbulent whether or not cavitation occurred. To take advantage of the cavitation number in cavitation prediction, it was compared with the negative coefficient of pressure to decide when cavitation was likely to occur.

4.2 Recommendations

Future research needs to consider two main issues: nozzle design and the measurement equipment. For the nozzle design, testing various levels of surface roughness for the insert is highly recommended, so as to observe the impact of surface roughness on cavitation formation. Testing several diverging angles will highlight its effect. Also, eliminating the vibration is important, to allow reducing the throat area, so as to get additional pressure drop; otherwise, the insert's vibration might break the glass.

For the measurement equipment, the refrigerant temperature needs to be measured right after the throat to investigate the temperature drop accurately. Because of the glass, installing a

thermocouple inside the tube would be a challenge. Using a thermal infrared might provide an acceptable temperature evaluation.

References

[1] http://www.iifiir.org/userfiles/file/webfiles/summaries/Refrigerant_classification_EN.pdf

[2] EPA certification exam preparatory manual

[3] http://dynarx.com/product/1112-tetrafluoroethane/

[4] Cengel, Yunus A., and Michael A. Boles. "Thermodynamics: an engineering approach." *Sea* 1000 (2002): 8862.

[5] http://www.eng.utah.edu/~lzang/images/lecture-10.pdf

[6] Yunus, A. Cengel, and John M. Cimbala. "Fluid mechanics fundamentals and applications." *McGraw-Hill Publication* 2 (2006).

[7] Schmidt, Aaron James. *Quantitative measurement and flow visualization of water cavitation in a converging-diverging nozzle*. Diss. Kansas State University, 2016.

[8] http://www.ffn.ub.edu/davidr/index.php?option=com_content&view=article&id=44:introduction-to-nucleation&catid=34:nucleation&Itemid=58

[9] Badday, Ali Sabri, et al. "Intensification of biodiesel production via ultrasonic-assisted process: a critical review on fundamentals and recent development." *Renewable and Sustainable Energy Reviews* 16.7 (2012): 4574-4587.

[10] https://archive.cnx.org/contents/a05a0ee3-8a56-43d0-b77d-d06263d15817@5/phase-diagrams

[11]https://www.thermalfluidscentral.org/encyclopedia/index.php/Phase_and_chemical_equilibrium

[12] Nazemi, E., et al. "Precise void fraction measurement in two-phase flows independent of the flow regime using gamma-ray attenuation." Nuclear Engineering and Technology 48.1 (2016): 64-71.

[13] https://en.oxforddictionaries.com/definition/blowdown

[14] Barrow, Gordon. Physical chemistry. New Delhi: McGraw-Hill Publishing, 1988

[15] Carey, Van P. "Liquid-vapor phase-change phenomena." (2008)

[16] Wilms, Jeffrey. *Flow visualization of cavitation*. Diss. Kansas State University, 2016.

[17] Alkotami, Abdulmalik. *An investigation of cavitation cooling effect in converging-diverging nozzles*. Diss. Kansas State University, 2016.

[18] Jablonská, Jana, and Marian Bojko. "Multiphase flow and cavitation-Comparison of Flow in Rectangular and Circular Nozzle." *EPJ Web of Conferences*. Vol. 92. EDP Sciences, 2015.

[19] Brennen, Christopher E. Fundamentals of multiphase flow. Cambridge university press, 2005.

[20] Brennen, Christopher E. Fundamentals of multiphase flow. Cambridge university press, 2005.

[21] https://www.britannica.com/science/halogen-element

[22] http://www.chemistryexplained.com/Ny-Pi/Organic-Halogen-Compounds.html

[23] Goetzler, William, et al. "Alternatives to vapor-compression HVAC technology." *ASHRAE Journal* 56.10 (2014): 12.

[24] Charamko, Serguei, Kristian Debus, and Tom Gielda. "Cooling system utilizing a reciprocating piston." U.S. Patent Application No. 13/087,062.

[25] Alkotami, Abdulmalik, et al. "A Thermodynamic Analysis of the Temperature Drop and Potential Cooling Effect of Cavitation." *ASME 2015 International Mechanical Engineering Congress and Exposition*. American Society of Mechanical Engineers, 2015.

[26] Asher, William. *Fluid dynamics of cavitating sonic two-phase flow in a converging-diverging nozzle*. Diss. Kansas State University, 2014.

[27] Wallis, Graham B. "One-dimensional two-phase flow." (1969).

[28] Lecoffre, Yves. *Cavitation: bubble trackers*. CRC Press, 1999.

[29] Ahmed, Zayed. *Quantitative Flow Measurement and Visualization of Cavitation Initiation and Cavitating Flows in a Converging-Diverging Nozzle*. Diss. Kansas State University, 2017.

[30] http://gerler-engineering.com/terminology/, visited on 6/4/2017

[31] Caupin, Frédéric, and Eric Herbert. "Cavitation in water: a review." *Comptes Rendus Physique* 7.9-10 (2006): 1000-1017.

[32] Franc, Jean-Pierre. *Physics and control of cavitation*. GRENOBLE UNIV (FRANCE), 2006.

Appendix A - High Speed Camera Specifications

Specifications: Partial Frame Rate / Recording Duration Table

FRAME RATE (fps)	MAXIMUM RESOLUTION Horizontal	Vertical	MAXIMUM SHUTTER SPEED	RECORD DURATION (12-BIT) TIME (Sec.) 8GB	16GB	32GB	64GB	FRAMES 8GB	16GB	32GB	64GB
1,000	1,024	1,024	1 µs 1/1,000,000 sec	5.46	10.92	21.84	43.68	5,457	10,918	21,841	43,686
2,000	1,024	1,024		2.73	5.46	10.92	21.84	5,457	10,918	21,841	43,686
4,000	1,024	1,024		1.36	2.73	5.46	10.92	5,457	10,918	21,841	43,686
5,000	1,024	1,024		1.09	2.18	4.37	8.73	5,457	10,918	21,841	43,686
7,000	1,024	1,024		0.78	1.56	3.12	6.24	5,457	10,918	21,841	43,686
7,500	1,024	1,000		0.75	1.49	2.98	5.96	5,588	11,180	22,365	44,735
9,300	1,024	800		0.75	1.50	3.01	6.01	6,985	13,975	27,956	55,918
10,000	1,024	744		0.75	1.50	3.01	6.01	7,511	15,027	30,061	60,127
15,000	960	528		0.75	1.51	3.01	6.02	11,289	22,587	45,182	90,374
20,000	832	448		0.77	1.54	3.07	6.14	15,352	30,716	61,443	122,898
30,000	768	320		0.78	1.55	3.11	6.21	23,284	46,586	93,189	186,396
50,000	512	272		0.82	1.64	3.29	6.57	41,090	82,211	164,452	328,934
75,000	320	264		0.90	1.81	3.61	7.22	67,737	135,523	271,097	542,244
100,000	320	192		0.93	1.86	3.73	7.45	93,138	186,345	372,758	745,585
150,000	256	144		1.03	2.07	4.14	8.28	155,230	310,575	621,264	1,242,642
300,000	256	64		1.16	2.33	4.66	9.31	349,269	698,794	1,397,845	2,795,946
420,000	128	64		1.66	3.33	6.66	13.31	698,538	1,397,589	2,795,690	5,591,893
525,000	128	48		1.77	3.55	7.10	14.20	931,384	1,863,452	3,727,587	7,455,857
775,000	128	24		2.40	4.81	9.62	19.24	1,862,769	3,726,904	7,455,175	14,911,715
930,000	128	16	369 ns 1/2,712,000 sec	3.00	6.01	12.02	24.05	2,794,154	5,590,357	11,182,762	22,367,573
1,000,000	64	16		5.59	11.18	22.37	44.73	5,588,309	11,180,714	22,365,525	44,735,146

OPTION SUBJECT TO EXPORT LICENSE CONTROL RESTRICTIONS WHERE APPLICABLE

Sensor	12-bit ADC (Bayer system color, single sensor) with 20µm pixel
Shutter	Global electronic shutter from 16.7ms to 1µs independent of frame rate
Lens Mount	Interchangeable F-mount and C-mount using supplied adapters
Extended Dynamic Range	Selectable in twenty steps (0 to 95% in 5% increments) to prevent pixel over-exposure
Memory	8GB (standard: 5,457 frames @ maximum resolution) 16GB (option: 10,913 frames @ maximum resolution) 32GB (option: 21,841 frames @ maximum resolution) 64GB (option: 43,686 frames @ maximum resolution)
Video Output 1	NTSC/PAL composite VBS (BNC). Ability to zoom, pan and tilt within image via keypad. Live video during recording
Video Output 2	HD-SDI: HD-SDI 2 channel (BNC) digital output
Camera Control	Through optional keypad with integrated viewfinder and Gigabit Ethernet or RS-422
User Preset Switches	Four user selectable camera function controls mounted on the camera's rear panel
Low Light Mode	Low light mode drops the frame rate and shutter time to their maximum values, while maintaining other set parameters, to enable users to position and focus the camera
Triggering	Selectable positive or negative TTL 5Vp-p or switch closure
Trigger Delay	Programmable delay on selected input and output triggers, 100ns resolution
Timing	Internal clock or external source
Phase Lock	Enables cameras to be synchronized precisely together to a master camera or external source, such as IRIG/GPS time codes
Event Markers	Ten user entered event markers mark specific events within the image sequence in real time. Immediately accessible through software
Dual Speed Recording	Enables the recording speed to be changed up or down by a factor of 2, 4 or 8 during a recording
Trigger Modes	Start, End, Center, Manual, Random, Random Reset, Random Center, Random Manual and Duals Speed Recording
Saved Image Formats	JPEG, AVI, TIFF, BMP, RAW, PNG, MOV and FTIF. Images can be saved with or without image or comment data
Data Display	Frame Rate, Shutter Speed, Trigger Mode, Date or Time, Status (Playback/Record), Real Time, Frame Count and Resolution
Partitioning	Up to 64 memory segments for multiple recording in memory
Data Acquisition	Supports Photron MCDL and DAQ
Cooling	Actively cooled
Operating Temperature	0 - 40 degrees C (32 - 104 degree F)
Mounting	1 x 1/4 - 20 UNC, 1 x 3/8 - 16 UNC, 6 x M6
Dimensions	165mm (6.50")H×153mm (6.02")W×242.5mm (9.55")D *excluding protrusions
Weight	6.2 kg (13.67 lbs)
Power Requirements	100V-240V AC ~ 1.5A, 50-60Hz DC operation 18-36 V DC, 100VA

References:
[1] http://photron.com/wp-content/uploads/2014/07/FASTCAM_SA5.pdf
[2] Wilms, Jeffrey. *Flow visualization of cavitation*. Diss. Kansas State University, 2013.

Appendix B - O-Ring Groove Standard

The following figures is screen shot of the standards that I used to select the O-ring groove dimensions. Figure 1 is to get the O-ring thickness. Depending on the thickness, the groove dimensions was selected.

O-Ring Size Chart

How to measure an O-Ring?

O-rings are actually really easy to measure. All you need to do is measure the internal diameter (ID) or outside diameter (OD) and the width or cross section (C/S) of the o ring. The diagram shows exactly where these dimensions are to be found. Once you have these measurements you then need to decide if the size you need is listed below or if the best fit will be a metric oring. Once you have the AS-568 dash size you need, select the compound link at the bottom of the page to place your order.

To calculate an o-ring's outside diameter (OD) you may use this formula: 2(CS) + ID = OD
If you have the OD and need to find the ID use this formula: OD - 2(CS) = ID

Link to order AS568 O-Rings online: **AS568 O-Rings**

AS568 O-Ring Size Chart

AS568A	NOMINAL SIZE (Inch)			Actual Size (Inch)		Actual Size (mm's)	
Dash No.	ID	OD	CS	ID	CS	ID (mm)	CS (mm)
-001	1/32	3/32	1/32	.029±.004	.040±.003	0.74±0.10	1.02±0.08
-002	3/64	9/64	3/64	.042±.004	.050±.003	1.07±0.10	1.27±0.08
-003	1/16	3/16	1/16	.056±.004	.060±.003	1.42±0.10	1.52±0.08
-004	5/64	13/64	1/16	.070±.005	.070±.003	1.78±0.13	1.78±0.08
-005	3/32	7/32	1/16	.101±.005	.070±.003	2.57±0.13	1.78±0.08
-006	1/8	1/4	1/16	.114±.005	.070±.003	2.90±0.13	1.78±0.08
-007	5/32	9/32	1/16	.145±.005	.070±.003	3.68±0.13	1.78±0.08
-008	3/16	5/16	1/16	.176±.005	.070±.003	4.47±0.13	1.78±0.08
-009	7/32	11/32	1/16	.208±.005	.070±.003	5.28±0.13	1.78±0.08
-010	1/4	3/8	1/16	.239±.005	.070±.003	6.07±0.13	1.78±0.08
-011	5/16	7/16	1/16	.301±.005	.070±.003	7.65±0.13	1.78±0.08
-012	3/8	1/2	1/16	.364±.005	.070±.003	9.25±0.13	1.78±0.08
-013	7/16	9/16	1/16	.426±.005	.070±.003	10.82±0.13	1.78±0.08
-014	1/2	5/8	1/16	.489±.005	.070±.003	12.42±0.13	1.78±0.08
-015	9/16	11/16	1/16	.551±.007	.070±.003	14.00±0.18	1.78±0.08
-016	5/8	3/4	1/16	.614±.009	.070±.003	15.60±0.23	1.78±0.08
-017	11/16	13/16	1/16	.676±.009	.070±.003	17.17±0.23	1.78±0.08
-018	3/4	7/8	1/16	.739±.009	.070±.003	18.77±0.23	1.78±0.08
-019	13/16	15/16	1/16	.801±.009	.070±.003	20.35±0.23	1.78±0.08
-020	7/8	1	1/16	.864±.009	.070±.003	21.95±0.23	1.78±0.08

Figure 4.1 O- ring Dimensions

Seal Types & Gland Design

One general guideline for good O-ring application and design is to maintain a range of % sqeeze on the O-ring (~10-40% for static and no more than 30% for dynamic).

No less than 75% of the seal cross-section should be contained within the groove to ensure the seal does not "roll" or extrude out of the groove. See Section 5 for more detail on determining the allowable clearance gap.

Finally, be sure to consider the void/volume relationship in worse case tolerance conditions. The maximum O-ring volume should not exceed 90% of the minimum gland void. The groove width may be increased to provide additional void.

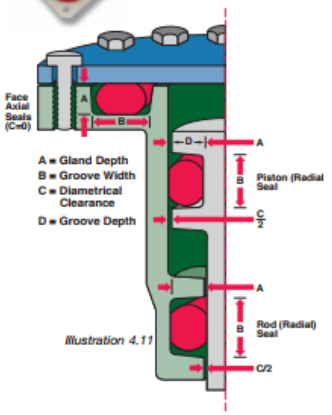

Table A — O-Ring Gland Design For Dynamic Seals

Note: Table A contains general sealing guidelines. More specific information is available throughout this guide.

O-Ring Cross Section	Gland Depth	Squeeze		Diametrical Clearance Max.	Groove Width. ±.005			Groove Radius	Eccen-tricity Max.
		Inches	%		No Backup Rings	One Backup Ring	Two Backup Rings		
.040	.031/.033	.004/.012	11-28	.004	.063	–	–	.005-.008	.002
.050	.039/.041	.006/.014	13-26	.004	.073	–	–	.005-.008	.002
.060	.047/.049	.008/.016	14-25	.004	.084	–	–	.005-.008	.002
.070	.055/.057	.010/.018	15-25	.004	.095	.150	.208	.005-.015	.002
.103	.087/.090	.010/.019	10-18	.005	.145	.187	.249	.005-.020	.003
.139	.119/.123	.012/.024	9-17	.006	.185	.222	.301	.005-.030	.004
.210	.183/.188	.017/.032	8.5-15	.006	.285	.338	.428	.005-.050	.006
.275	.234/.240	.029/.047	10.5-17	.007	.375	.440	.579	.005-.060	.008

O-Ring Gland Design For Static Seals

O-Ring Cross Section	Gland Depth		Squeeze				Dia-metrical Clearance Max.	Groove Width. ±.005			Groove Radius	Eccen-tricity Max
			Radial →O←		Axial O			No Backup Rings	One Backup Ring	Two Backup Rings		
	Radial	Axial	Inches	%	Inches	%						
†.020	.013-.014	.013-.014	.004-.009	22-41	.004-.009	22-41	.002	.035	–	–	–	.0015
.030	.020-.022	.020-.022	.005-.013	19-39	.005-.013	19-39	.003	.045	–	–	–	.0015
.040	.027-.030	.027-.030	.007-.016	19-37	.007-.016	19-37	.003	.060	–	–	.005-.008	.002
.050	.035-.039	.034-.038	.008-.018	17-34	.009-.019	19-36	.004	.075	–	–	.005-.008	.002
.060	.042-.047	.042-.046	.010-.021	18-33	.011-.021	19-33	.004	.090	–	–	.005-.008	.002
.070	.050-.055	.049-.054	.012-.023	18-32	.013-.024	19-33	.004	.105	.150	.208	.005-.015	.002
.103	.080-.086	.075-.081	.014-.026	14-25	.019-.031	19-29	.005	.146	.182	.244	.005-.020	.003
.139	.110-.116	.100-.108	.019-.033	14-23	.027-.043	20-30	.006	.195	.217	.296	.005-.030	.004
.210	.170-.176	.155-.165	.029-.045	14-21	.040-.060	20-28	.006	.280	.333	.423	.005-.050	.006
.275	.225-.235	.205-.215	.034-.056	13-20	.054-.076	20-27	.007	.350	.435	.574	.005-.060	.008

†Note: It is recommended that an O-ring with tighter CS tolerance (±.002) be requested.

www.applerubber.com
1.800.828.7745 (US & Canada Only) • +1.716.684.6560 (International)

Figure 4.2 O- ring's groove Dimensions [2]

References

[1] http://www.theoringstore.com/index.php?main_page=page_2

[2] http://www.applerubber.com/src/pdf/seal-design-guide.pdf